fire

MDPI

Review

Advances in Detection and Monitoring of Coal Spontaneous Combustion: Techniques, Challenges, and Future Directions

Lucica Anghelescu and Bogdan Marian Diaconu *

Faculty of Engineering, "Constantin Brancusi" University of Targu Jiu, Calea Eroilor 30, 210135 Targu Jiu, Romania; lucica.anghelescu@e-ucb.ro
* Correspondence: bogdan.diaconu@e-ucb.ro

Abstract: Coal spontaneous combustion (CSC) is a multifaceted research domain that has been widely explored in the literature, ranging from analytical and numerical modeling to the development of fire suppression materials and methods. A comprehensive review of the literature has revealed several distinct research trajectories, or "roadmaps", identified through criteria such as the volume of studies addressing each theme, the presence of review papers dedicated to a specific roadmap, and the explicit mention of coal spontaneous combustion in the title or keywords. This classification framework has outlined six primary roadmaps: (1) spread, quantification, and impact; (2) mechanisms, models, factors, and parameters; (3) experimental studies and models; (4) detection, monitoring, and prediction; (5) prevention and control; and (6) applications. While interconnections exist between these roadmaps, and all ultimately converge towards roadmap 5 (prevention and control), each roadmap constitutes a distinct research cluster. The focus of this review is on roadmap 4, specifically addressing the methods and technologies for detection, monitoring, and prediction of CSC events. This review encompasses studies published from 2010 to the present, providing a thorough examination of the various detection techniques employed, with particular emphasis on their limitations and the strategies proposed to overcome these challenges. A critical analysis highlights the key advantages and disadvantages of each category of techniques, offering insights into their practical applications and the potential for future advancements in this field. The present review aims to contribute to the refinement of detection and monitoring methods for CSC, with the goal of enhancing early detection capabilities and improving fire management strategies.

Keywords: coal spontaneous combustion; detection techniques; gas monitoring; ground temperature measurement; thermal infrared imaging; remote sensing

Citation: Anghelescu, L.; Diaconu, B.M. Advances in Detection and Monitoring of Coal Spontaneous Combustion: Techniques, Challenges, and Future Directions. *Fire* **2024**, *7*, 354. https://doi.org/10.3390/fire7100354

Academic Editor: Thomas H. Fletcher

Received: 15 September 2024
Revised: 2 October 2024
Accepted: 3 October 2024
Published: 5 October 2024

1. Introduction

Spontaneous combustion is a class of combustion processes triggered by a temperature increase caused by exothermic chemical and physical phenomena. In general, it is agreed that spontaneous combustion has two phases: (i) The slow phase, during which the reaction rate is low and the whole mass of material heats up almost uniformly. The heat is dissipated at the interface with the environment by various heat transfer mechanisms, mainly convection. Depending on the thermal equilibria conditions, the process can be slowed down or it can evolve and reach the second phase. (ii) The thermal runaway phase, in which the exothermic internal reaction speeds up due to the temperature increase and create an avalanche effect. The temperature increase rate becomes extremely high and eventually autoignition occurs.

Both inorganic and organic materials can undergo spontaneous combustion, but with different triggering mechanisms. Coal is an organic material with a significant spontaneous combustion potential, which is a key hazard in coal mines. Spontaneous combustion of coal is a complex process influenced by many factors, either directly or through a chain of triggering processes. Coal spontaneous combustion occurs in coal stockpiles, coalfields,

underground mines, and, in general, whenever coal is stockpiled for long periods. The spontaneous combustion of coal causes economic losses, generates greenhouse gases and poses risks to property through the spread of fire. Coal fires caused by spontaneous combustion have two distinctive features compared to conventional fires:

1. Coal fires can develop in underground seams as smoldering combustion, representing some of the most persistent fires on Earth, with occurrences dating back several million years, as noted by Heffern and Coates [1]. These fires are notoriously difficult or even impossible to extinguish, leading to both immediate, observable consequences such as wildfires, and longer-term, less predictable impacts like the alteration of adjacent geological formations. The terrain-shaping effects of coal fires have been documented in a study by Heffern and Coates [1].
2. Coal fires do not always require an ignition source. Once the thermal runaway threshold temperature is reached, the coal mass ignites spontaneously. The thermal runaway threshold can be anywhere between 80 and 120 °C (Song et al. [2]) depending on many factors.

A bibliometric analysis on the topic of coal spontaneous combustion was carried out by Liu et al. [3]. The analysis included metrics such as the number of publications over time, the countries/regions and organizations from where the publications originated, the journals, and various domain maps discussing the keywords spontaneous combustion, spontaneous ignition, self-ignition, self-heating and pyrophoric. A key conclusion derived from this study is that spontaneous combustion research is a multidisciplinary domain, integrating knowledge from areas such as fuel science, chemistry, thermodynamics, heat and mass transfer.

Another bibliometric analysis was conducted by Yang and Qiu [4]. The following list of terms contained in either title, abstracts, and keywords list, was used to extract from Science Citation Index Expanded publications from 1984 to 2018: coal spontaneous combustion, coal self-heating, coal spontaneous heating, coal low-temperature oxidation. A number of 829 publications were selected, out of which 91.31% were journal articles. The bibliometric analysis reported in this paper focused mainly on the following issues:

- ➢ Originating geographic area of the publications. The top four positions were occupied by China with 348, followed by Australia with 96, USA with 92 and India with 45 publications. China is far ahead of the pack, which is explained by the high prevalence of coal fires.
  Note: A significant number of coal seams, particularly in the regions Xinjiang and Inner Mongolia, meet the geological conditions and mining practices to render them highly susceptible to fire, Huang et al. [5]. Coal fire cause annual losses exceeding 100 million ¥, spontaneous combustion fires accounting for 90–94% of the total fire events in mines [5]. Huang et al. [5] present a statistic (without mentioning the source of the figures) stating that 32 underground coal spontaneous combustion or gas explosion accidents occurred in China between 2001 and 2014, causing 614 deaths.
- ➢ Journals having published papers on the topic of CSC.
- ➢ Keyword occurrence. The top four keywords and their respective occurrence frequency values were low temperature oxidation (353), coal spontaneous combustion (302), coal (169) and mine fire (137). The keyword with the highest occurrence frequency can be explained by the fact that low temperature coal oxidation is the triggering factor that ultimately results in coal spontaneous combustion. Other keywords related to chemical interaction between coal and molecular oxygen were encountered, such as kinetics, mechanism, model and particle size. Keywords related to prevention and control such as prevention (37), prediction (26) and inhibitor suggest the existence of a consolidated research direction.

Onifade and Genc [6] conducted a review on the topic of "spontaneous combustion of coal". The content of this review is limited to three sections, mathematical modelling, exper-

imental methods and statistical methods. The article has a narrative structure summarizing several works, selected on unspecified criteria.

Zhang et al. [7] conducted a review on numerical studies on the topic of self-heating of a coal stockpile. A bottom-up approach has been employed in structuring the article discussing first the mechanisms of coal stockpile self-heating, the transfer equations and the constants used by various authors, a section dedicated to the variables (coal and stockpile characteristics, moisture and wind) and concluding with a section describing the main findings: the simple Arrhenius dependence on defining the coal oxidation rate is an acceptable approach after the occurrence of the thermal runaway but not at low temperatures; the Arrhenius parameters change with the particle; the reviewed studies are not consistent in assessing the effect of the coal particle size on the dynamics of the coal stockpile self-heating; three distinct stages were identified in the temperature profile: an initial slow rise due to the self-heating, a plateau phase which was explained by the energy expenditure to support the phase transition of water, and a third, steep-gradient stage, explained by the fast oxidation of dry coal. Song and Kuenzer [8] reviewed the literature on the coal fires occurring in China a decade back (from the date the article was published). It was reported that written evidence of coal fires dates as early as 386–534 AD. Coal fire distribution and development were discussed and some theories were put forward to explain the occurrence of coal fires in the north of China. A significant section of the article discusses issues related to detection and monitoring of coal fires. The detection and monitoring methods were grouped into four categories, as follows: underground, ground, airborne and space remote sensing methods. Three other sections were included discussing modelling of underground fires, environmental impact and fire control techniques.

In general, reviews covering the larger topic of CSC cannot thoroughly discuss all the components of the problem. For this reason, recent reviews focus on more narrow issues connected to the ultimate goal of the CSC research, that is prevention and control. Two sub-topics were identified where significant research has been published and several reviews were conducted:

1. Theoretical background, analytical models and numerical studies of the self-heating coal stockpiles and self-ignition are a set of issues of importance in designing prevention and control techniques. A comprehensive review on the topic of CSC hazard assessment based on thermal-kinetic and heat and mass transfer was carried out by Lu et al. [9]. The large volume of literature on this topic was divided into several sections: propensity rating for coal spontaneous combustion with small loading, fire potential for coal spontaneous combustion based on large-scale approach, and field investigation. This division is significant in understanding the main research directions pertaining to the CSC. Several key conclusions defining the need for more in-depth research were formulated: extrapolating small-scale indices, such as self-heating rate, heat release intensity, oxygen consumption, as well as dimensionless parameters, to large and/or full-scale models has not been fully validated; the macroscopic approach used in current mathematical modelling of CSC are not always consistent with the measured data, the development of a multiscale modelling methodology is highly desirable; although the existence of a threshold between self-sustaining and extinction conditions for coalfield fire has been established, more research is required to define quantitatively the threshold conditions. Studies employing numerical solutions for the self-heating of the coal stockpiles and spontaneous combustion were reviewed by Zhang et al. [7]; a short discussion on the topic of mathematical models and factors that determine the dynamics of the self-heating process was included in the general review conducted by Onifade and Genc [6].
2. Mechanisms and methods for prevention and control of CSC is actually the ultimate goal of research in this direction. Li et al. [10] conducted a review discussing the most prevalent materials used in prevention of CSC. The mechanisms by which the inhibitors slow down or suppress the chemical and physical processes leading ultimately to CSC were discussed and a classification of materials was carried out

based on the inhibition mechanism. The availability, cost and environmental impact of inhibitors were assessed. The techniques, methods, and materials applied in the prevention of coal spontaneous combustion were reviewed in Onifade [11] (measures), Kong et al. [12] (methods to prevent CSC), Han et al. [13], and Lu et al. [14] (fire prevention materials), and Dai et al. [15] (heat pipe systems to prevent CSC in coal storage piles).

2. Research Methodology

A Scopus search from 2010 to date including document type article, conference paper, review, conference review resulted in 1176 documents using the keyword "coal spontaneous combustion". The Scopus search was limited to the "Keyword" field. A bibliometric analysis by means of VOS Viewer reported an author keywords number of 2119. We set the following filters as follows: Document type to Article, Conference paper and Review, Language to English, and Source type to Journal and Conference proceeding, the total number of entries was reduced to 928. In the VOS Viewer tool, the number of keyword occurrence was set to the default value 5, resulting a number of 91 keywords. The list of keywords contained entries with high semantic similarity (e.g., "coal spontaneous combustion" and "spontaneous combustion of coal") which were not removed since the main purpose of this analysis was to identify/define the main research directions in CSC. The top five keywords semantically distinct were "coal spontaneous combustion" with 576 occurrences, "activation energy"—38, "characteristic temperature"—34, "coal"—44, and "apparent activation energy"—29. An initial manual screening was performed, first based on titles and then on abstracts, to define research roadmaps. The criteria for defining a roadmap topic were as follows:

1.1 A minimum number of 20 studies broadly discussing a topic define a research roadmap.
OR
1.2 At least one review article was identified.
AND
2. The coal spontaneous combustion is mentioned in the title, keywords, or abstract.

In defining the roadmaps, some degree of topic disjunction was sought, in the sense that the roadmap classification would become less meaningful if two or more topics would merge.

Six roadmaps were identified as follows:

1. Spread, quantification and impact
These are mainly experimental studies and field reports discussing:
   - 1.1 General characteristics, specific features, morphology and large-scale effects of coal fires occurring throughout the world: Song and Kuenzer [8], Kuenzer et al. [16], Saini et al. [17], Kuenzer and Stracher [18], Kus [19], Xu et al. [20], etc.
   - 1.2 Coal fires as a source of pollution and environmental impact: Li et al. [21], Carroll et al. [22], Oliveira et al. [23], Deng et al. [24], etc.
2. Mechanisms, models, factor and parameters
This category includes
   - 2.1 Studies advancing analytical models for self-heating of coal and spontaneous combustion: Lu et al. [9], Xia et al. [25], Rua et al. [26], Xi et al. [27], Xiao et al. [28], etc.
   - 2.2 CFD studies presenting numerical simulation of the coal self-heating and CSC as well as the influence of physical factors: Yuan et al. [29], Taraba et al. [30], Chen et al. [31], Zhuo et al. [32], Xiaomeng et al. [33], etc.
   - 2.3 Parametric studies investigating the influence of physical factors (wind, moisture content, particle size) and chemical (coal grade, presence of foreign com-

pounds, etc.): Zhang et al. [34], Yu et al. [35], Plakunov et al. [36], Qiao et al. [37], Deng et al. [38], Zhang et al. [39], Zhang et al. [40], Li et al. [41], etc.

2.4 Studies relying on artificial intelligence models and nature-inspired algorithms, primarily aimed at assessing the propensity of coal spontaneous combustion: Said et al. [42], Lei et al. [43], Sahu et al. [44], Xie et al. [45], Li et al. [46], Sahu et al. [47], Wang et al. [48], etc.

3. Experimental studies and models
A class of studies attempting to investigate experimentally the CSC and validate numerical models:

3.1 The dynamics and susceptibility of CSC: Li et al. [49], Onifade et al. [50], Wen et al. [51], Zhang et al. [52], Yan et al. [53], Zhao et al. [54], etc.

3.2 Fire control methods and materials: Fan et al. [55], Zhang et al. [56], Zhang et al. [57], Cheng et al. [58], etc.

3.3 In situ measurements and tests: Liu et al. [59] and Tang et al. [60].

4. Detection, monitoring and prediction
This category includes studies from the following sub-categories:

4.1 Methods for predicting or assessing the risk of coal self-combustion (CSC) in various systems, including coal stockpiles, coal seams, coal goafs, and coal gobs, both in underground and surface mining: Hu et al. [61], Song et al. [2], Du et al. [62], Wei et al. [63], Ma et al. [64], etc.

4.2 Detection of coal fires after the ignition phase using various methods, both direct and indirect, including secondary effects such as gas emissions: Guo et al. [65], Guo et al. [66], Gao et al. [67], Zhou et al. [68], etc.

4.3 Monitoring of existing and developing fires: Biswal and Gorai [69], Wang et al. [70], Hu et al. [71], Kong et al. [72], etc.

5. Prevention and control.

5.1 Techniques for CSC prevention: Liu et al. [73], Liu et al. [59], Shi et al. [74], Zhai et al. [75], etc.

5.2 Materials and methods for extinguishing the coal fires: Cheng et al. [76], Cheng et al. [77], Fan et al. [78], Li et al. [79], etc.

6. Applications

This research direction is relatively new, arising from the observation that certain coal fires are inextinguishable. Consequently, technologies have been developed to harness the thermal energy released by these fires: Shi et al. [80], Su et al. [81], Xiao et al. [82], Xiao et al. [83], etc.

It is important to observe that numerous studies span multiple research roadmaps. This overlap is expected, as the criteria for categorizing a study under a single roadmap can be inherently subjective. Review studies that specifically address or include at least one roadmap topic in a dedicated section were identified accordingly are presented in Table 1 (comprehensive overviews of coal spontaneous combustion and brief reviews are not included).

The detection, monitoring, and prediction of coal spontaneous combustion (CSC) are essential for managing and mitigating the risks posed by coal fires, which can cause extensive environmental damage, release hazardous emissions, and disrupt mining operations. Detection methods primarily aim to identify early-stage combustion events, where low-temperature oxidation occurs below the surface, often without visible signs. Techniques such as thermal infrared (TIR) imaging, gas emissions monitoring, and multispectral and hyperspectral sensors are widely employed to detect heat anomalies, volatile gases, and changes in the physical properties of coal and surrounding materials. Monitoring methods, on the other hand, focus on tracking the progression and spread of established fires, often using aerial and satellite-based remote sensing platforms to map fire boundaries, assess subsurface smoldering, and evaluate the effectiveness of fire suppression efforts.

Table 1. Review papers addressing fully or partially the roadmap themes.

Roadmap Theme	Author and Ref.	Year	Estimated Percentage Covering the Roadmap Theme
Spread quantification and impact	Song et al. [8]	2014	25
Mechanisms, models, factor and parameters	Song et al. [8] Lu et al. [9] Zhang et al. [7]	2014 2022 2016	12 100 100
Experimental studies and models	None identified	Not applicable	
Detection, monitoring and prediction	Song et al. [8] Liang et al. [84]	2014 2019	12 100
Prevention and control	Li et al. [10]	2020	100
Applications	Xiao et al. [82]	2023	100

Predictive modeling is also a critical component of CSC management, as it helps anticipate fire behavior by simulating parameters such as combustion depth, temperature gradients, and fire propagation rates. These models rely on field data obtained from detection and monitoring efforts, enabling the identification of high-risk areas and informing targeted intervention strategies. Despite advancements in these technologies, challenges remain, particularly in adapting detection techniques to varying geological and environmental conditions, ensuring continuous monitoring, and improving the accuracy of early-stage CSC detection. This review focuses on recent developments in CSC detection, monitoring, and prediction methods, evaluating their practical applications and highlighting key limitations and areas for further research.

3. Coal Spontaneous Combustion Detection

Coal fires, whether fully developed or in the developing phase, can be detected using a wide variety of methods and sensory systems. Accurate and timely detection is essential for any coal spontaneous combustion (CSC) detection technique. The selection of an appropriate technique depends primarily on the general layout and specific site conditions. More precise detection can be achieved by combining multiple techniques, leveraging the strengths of each while compensating for their limitations.

Three comprehensive CSC detection categories will be introduced in this review, as follows:

- Gas emission assessment
- Ground measurements
- Remote sensing

3.1. Gas Emission Assessment

3.1.1. Index Gases

Self-ignition of coal, either in coal stockpiles, seams or gobs, is the result of the oxidation exothermic process. Three stages were identified in the kinetics of the CSC by Dong et al. [85]: slow oxidation, accelerated oxidation and intense oxidation. Different kinds of gas products with different concentrations are released during each phase. The slow oxidation stage is the most complicated process, according to Xueqiu et al. [86], with low to moderate CO and CO_2 emissions at a constant rate until 150 °C, as presented in an experimental study performed by Dong et al. [85]. Between 150 and 180 °C, the emission rate starts to increase. At 180 °C, the concentrations of CO and CO_2 rise rapidly, indicating that the coal oxidation reaction has entered an accelerated stage. Guo et al. [66] reported slightly different values: the CO emission rate started to increase rapidly above 60 °C. This

value creates the conditions for the formation of coal–oxygen complexes. After 130 °C, the CO formation rate is even higher. The temperature threshold above which the rate of CO formation increases rapidly can be used as a marker of the rapid oxidation process and so to predict the inception of the spontaneous combustion. The emission of hydrocarbons is another important marker of ongoing oxidation processes. In an experimental study, Guo et al. [66] reported that the CH_4 emission is minimal below 100 °C (for long flame coal) and 80 °C (for anthracite). In fact, the CH_4 emission rate decreases slowly as the temperature increases. This is explained by the fact that the CH_4 emission consists of desorption of the CH_4 adsorbed in the coal pores. At temperature values varying between 100 and 140 °C, the CH_4 emission rate starts to increase, this being caused by the break of the side chains in the coal molecules. The temperature at which the methane production rate reverses indicates the onset of an oxidative process according to Zhao et al. [87]. In the same experimental study on CSC gas emissions conducted by Zhao et al. [87], it was reported that C_2H_4 was not present in coal samples below 100 °C. This is an indication of the fact that C_2H_4 does not exist in the raw coal and it is actually a result of the oxidative processes, according to Zhao et al. [87]. Another hydrocarbon commonly associated with coal oxidative processes is C_2H_6. Guo et al. [66] reported that C_2H_6 can be detected at temperatures as low as 20–30 °C, suggesting that trace amounts are adsorbed by the raw coal. Unlike C_2H_4, which is an unsaturated compound (Guo et al. [66]), C_2H_6 can be deposited in geological formations like coal seams, where it is more stable than C_2H_4, according to Liang et al. [84]. For this reason, the C_2H_6 presence cannot be used to predict the slow oxidation phase.

For any coal rank, the oxidative processes result in the production of CO, CO_2, CH_4, C_2H_4 and C_2H_6. The generation paths for hydrocarbons are complex (Liang et al. [84]) consisting of oxidation of functional groups and decomposition of stable complexes under the effect of the heat. It must be noted though that details of these reactions are not fully understood (Liang et al. [84]). Given the complex nature of gas emission dynamics during oxidative processes leading to coal spontaneous combustion (CSC), selecting an index gas to indicate key milestones in the process chain must consider sensitivity, detection feasibility, and consistency, according to Zhao et al. [87]. A summary of gas kinds used as indicators of CSC has been compiled by Liang et al. [84]. Detection of CSC based on index gases can be categorized into single gas and composite index detection techniques. Single gas techniques detect CO, which is the most important product of coal low-temperature oxidation. Other techniques are based on detection of hydrogen, Cliff et al. [88], or ethylene, Xie et al. [89]. Composite index gas techniques for detecting CSC involve analyzing a combination of gas species emitted during the low-temperature oxidation and combustion processes. These techniques are based on the principle that monitoring the ratios or composite indices of multiple gases enhances detection accuracy by integrating the concentration patterns of several species, rather than relying on a single indicator. This approach allows for more sensitive and reliable detection, as it accounts for variables such as coal rank, temperature, and environmental factors that may influence gas emissions. A summary of the single gas and composite gas index methods is presented in Table 2.

In practical applications, several factors inherent to the mining environment can compromise the performance of CSC detection systems, leading to either false positives (erroneous alarms) or undetected CSC events. Table 3 provides an overview of the common conditions that impact gas emission-based CSC detection systems and the methodologies employed to address these limitations.

Table 2. CSC detection based on gas concentration measurement. Single gas and composite index methods.

Single Gas	Advantages/Specific Features	Problems and Limitations	Used in
CO C_2H_4 C_2H_2 H_2	CO is a very effective indicator of early stages of low temperature oxidation. Monitoring techniques are available that can detect trace amounts of CO. CO has a density lower than the dry air, which stimulates the diffusion into the surrounding gases. C_2H_4 can serve as a useful signature gas for detecting CSC, as its presence is not associated with other known processes.	The absolute concentration of detected CO provides limited information about the fire status, whereas an increasing trend in CO production typically indicates a worsening fire condition. However, trend analysis alone cannot distinguish whether the CO is generated from widespread low-temperature coal oxidation or intense heating in a localized area. Air or other gases can dilute the index gas below the detection limit. In a less severe scenario, dilution can result in an underestimation of the heating state. Other gas sources (thermal engines emissions, seam gases) can contaminate the index gas. The intensity of heating cannot be determined solely based on the concentration of a single gas. H_2 may also be the product of the reaction of galvanized steel and acidic water during the sampling process. C_2H_4 is not an early indicator as it does not occur before 1500 °C.	Wen et al. [51] Qing et al. [90] Hu et al. [61] Ma et al. [91] Yang et al. [92]
Composite index:			
CO Make [93]. Defined as the CO volume flowing past a fixed point per unit time: $COMake = K \times CO \times Q\left[\frac{liters}{min}\right]$ K = 0.06 if CO is measured in ppm K = 600 if CO is measured in % $Q\left[\frac{m^3}{s}\right]$ airflow rate CO monoxide carbon concentration Typical values: >10 liters/min: investigation required >20 liters/min: significant fire danger >30 liters/min: extreme fire danger	Removes the effect of air dilution.	It cannot be used behind seals or in closed boreholes since it requires a continuous airflow. This limits significantly its applicability.	Liu et al. [94]
Graham's Ratio [93]. The percent change in CO concentration to change in O_2 concentration: $GR = \frac{100 \times CO}{0.256 \times N_2 - O_2}$ Typical values: <0.4: Normal 0.4–1.0: Uncertain (investigation required) 1.0–2.0: Heating >2: Intense heating or fire	Graham's Ratio is primarily utilized for detecting heating events or fires that might be obscured by variations in ventilation and for monitoring their progression over time. The trend in the ratio readings is of greater significance than the absolute values. An upward trend indicates a rise in temperature.	May underestimate the state of progression.	Xu et al. [95]
Young's ratio [93]: $YR = \frac{CO_2}{0.256 \times N_2 - O_2}$	No universal trigger levels can be established due to the significant variation in CO_2 generation with temperature across different coal ranks. The trend in the CO_2 ratio is more informative than the absolute values.	Other CO_2 sources—seam gas or thermal engines or CO_2 loss (dissolved in water) may influence the value.	Danish and Onder [96] Singh et al. [97]
CO/CO_2 ratio [93]: <0.02: Normal <0.05: coal temperature <60 °C <0.10: coal temperature <80 °C <0.15: coal temperature <100 °C <0.35: coal temperature <150 °C	Independent of oxygen deficiency. Increases rapidly during the early stages of heating. At high temperatures, the rate of increase reduces significantly.	Only intended as an early warning for heating. Other CO_2 sources from seam gas or vehicle exhaust may influence the value The potential loss of CO_2 as it readily dissolves in water. Can only be employed where no CO_2 emissions from other sources exist.	Yan et al. [98] Lu et al. [99] Wang et al. [100] Li et al. [101]

Table 2. *Cont.*

Single Gas	Advantages/Specific Features	Problems and Limitations	Used in
Morris Ratio [93]: $MR = \frac{N_2 - 3.774 \times O_2}{CO + CO_2}$	Valid in early stages of heating when increasing trend indicates increasing heating activity.	MR increases to a maximum at approximately 120 °C then decreases. The size of the peak varies with the coal rank.	Singh et al. [97]
Jones-Trickett Ratio [93]: $JTR = \frac{CO_2 + 0.75 \times CO - 0.25 \times H_2}{0.265 \times N_2 - O_2}$ Milestone values: <0.4 Normal conditions <0.5 Methane fire indication <1.0 Coal fire possible >1.6 Impossible	Increasing ratio indicates intensifying heating/temperature increase. Milestone values allow objective conclusions. Dilution with fresh air of the combustion products has no effect on the ratio.	Invalid if the intake air is oxygen deficient through the injection of nitrogen or carbon dioxide.	Singh et al. [97]
Litton Ratio [93]: $LR = \frac{1}{3} \times CO \times (\%Rg)^{-1.5} \times (\%O_2)^{-0.5}$ CO Carbon monoxide concentration in ppm $\%O_2$—Oxygen concentration in percent %Rg—residual gas in percent, defined as: $\%Rg = 100 - 4.774 \times O_2 - seamgas$ >1 Combustion process <1 and stable: Safe conditions <1 and decreasing: Equilibrium conditions not reached	Milestone values allow objective conclusions.	Can only detect the combustion but it is not sensitive enough to identify the initial phase of low-temperature oxidation.	Singh et al. [97]
Willet Ratio [93]: $WR = \frac{CO_2 \text{ produced}}{\text{Blackdamp} + \text{Combustibles}}$ No specific/milestone values defined	A falling trend suggests decreasing activity. Stable values may indicate no activity. More effective than Graham's Ratio in determining the state of spontaneous combustion activity behind sealed areas.		Singh et al. [97]
H_2/CO Ratio [93]	An increasing ratio indicates intensifying heating. Independent of dilution with fresh air, seam gas or oxygen deficiency.	CO can be depleted by bacterial activity. Thermal engine emissions can modify the trend. Rate of change slowed in sealed areas resulting in averaged values instead of instantaneous. Inaccurate for low H_2 values due to detection limitations.	
Ratio between hydrocarbons [93]: C_2H_6/C_2H_4 C_2H_6/CH_4 C_3H_8/CH_4 C_4H_{10}/CH_4 C_3H_8/C_2H_6 C_4H_{10}/C_2H_6		Hydrocarbons are produced at higher temperature and cannot be used to indicate the early stages of low-temperature oxidation.	

Table 3. Common issues in CSC detection via gas concentration measurement and proposed solutions.

Issue	Reference	Proposed Approach and Solution
Influence of the goaf atmosphere composition on the formation of index gases/composite index.	Liu et al. [102] 2021	The low-temperature oxidative process in a lean-oxygen atmosphere caused by the presence of CH_4 delays the formation of CO, CO_2, H_2 and C_2H_6. The temperature milestones for the occurrence of the gaseous components indicating CSC were modified in the presence of methane. For temperature values below 170 °C the composite index CO/CO_2 was not significantly influenced by the O_2 concentration and it can be determined with: $\frac{CO}{CO_2} = -0.675 + 0.333 \times e^{0.0257T}$ For temperature values above the 170 °C threshold, the presence of CH_4 and N_2 in the goaf atmosphere rendered the CO/CO_2 irrelevant for the indication of CSC

Table 3. *Cont.*

Issue	Reference	Proposed Approach and Solution
Ventilation air dilution lowers the index gas concentration (C_2H_4, CO) below the detection limits of the instruments.	Xie et al. [89] 2011	A C_2H_4 enriching system was proposed consisting of a gas flow system, a C_2H_4 enriching and adsorption system, a temperature control system and a gas detection system. It was reported that C_2H_4 detection sensitivity increased by approximately 10 times. Field application of the EES at two coal mines demonstrated that the detection of ethylene was accelerated by 2 to 3 weeks.
Threshold concentration values may be relative and misleading in some environments and conditions.	Liu et al. [94] 2024	Temperature and CO concentration was measured in the air return roadway in two points: close to the working surface and at a distance of 16 m. A relationship between the temperature and CO concentration at the two points was established to determine the statistical patterns between the two variables. Eventually, a relationship was established between the measured CO concentration in the air return roadway and the critical concentration in the goaf.
CSC stages cannot be precisely and timely identified using the standard index gas or composite index.	Ma et al. [64] 2020	A controlled CSC experiment was designed using coal samples from Huainan mining area, China. A new index—the oxidation index—was proposed for predicting coal spontaneous combustion, defined as the ratio of oxygen consumption per unit time to the total oxygen consumption. Threshold values for the oxidation index were identified to indicate the transition between stages.
	Zhang et al. [103] 2021	Six characteristic temperatures and their corresponding threshold values were determined, allowing the coal spontaneous combustion process to be divided into seven stages: the latent stage, recombination stage, self-heating stage, activation stage, thermal decomposition stage, fission stage, and combustion stage.
	Cheng et al. [104] 2022	A critical CO concentration value was defined based on temperature, gob geometry and gob ventilation conditions.
	Yan et al. [98] 2023	Optimized indexes for temperature ranges consisting of ratios of different alkanes were defined.
Mining environment factors alter the gas sensor signal or sensor failures occur.	Chang and Chang [105] 2023	Gas concentration data were converted into recurrence plots [106]. By means of deep learning-based image feature engineering (VGG16, VGG19, and ResNet18), the temporal features of gas concentration time series were converted into image format. This approach enables the representation and comparative analysis of sensor monitoring data from different locations, facilitating the identification of operational status and anomalies.

3.1.2. Radon Gas Emission

Radon exhalation of coal is a complex process, which is has been observed and documented but no analytical model has been proposed to date. The energy recoil generated by radium (the parent nuclide of radon) represents the acting force that causes the migration of radon. The recoil energy causes the radon atoms to come loose from the shackles of the mineral lattice and move freely. Some of the newly freed radon atoms penetrate the pore space of the coal, through which a migration process begins. The migration is favored by the cracks in the coal structure, connected to the surface. The diffusion process is driven by the concentration and pressure gradients.

The radon release has two distinct stages, Lu et al. [107], Zhou et al. [108], Wen et al. [109]:

1. Some radon atoms are absorbed and captured in the internal pores of the coal and others are held captive in the water-filled pores because the transport range of radon in the water is considerably smaller than in air. The exothermic oxidation reaction causes the vaporization of porous water and the radon atoms are released into the external environment.
2. As the temperature increases, the pyrolysis process causes the closed pore of the coal to collapse and connect and in the same time new crack paths to the environment are created. The thermal diffusion and convection cause the radon atoms to migrate through these paths.

Observations show that the radon concertation increases linearly until 50–70 °C. After these values, a sharp increase in the exhalation rate occurs. Between 100 and 120 °C, the radon exhalation rate remains steady. A numerical study modelling the radon exhalation process occurring was carried out by Lu et al. [107] considering the permeability of the goaf (and its dependence on the crushing coefficient), the momentum and energy conservation equation, and species conservation equation, considering the radon decay term. It was reported that CSC in the goaf induces a porous chimney effect, characterized by thermal buoyancy and vortex formation in the high-temperature region. The thermal buoyancy effect arises from the increase in coal temperature, which reduces gas density in the affected area. This density reduction generates a vertical upward buoyant flow. Concurrently, the decreased gas density creates an apparent local negative pressure in the combustion zone, leading to vortex formation around the area due to the suction effect of the negative pressure. The porous chimney effect offers a theoretical framework for understanding radon source formation in the goaf. The distribution of radon in the goaf results from the two concurrent processes, air leakage and the porous chimney effect. During the low-temperature stage of coal, air leakage predominates, causing radon to accumulate near the air return side. As coal temperature rises, the porous chimney effect becomes dominant. The updraft generated by thermal buoyancy rapidly transporting radon to the top of the goaf. The vortex-induced fresh airflow supplies both oxygen and radon to the high-temperature zone of coal spontaneous combustion. Once heated, this airflow re-establishes an upward buoyant flow, further intensifying radon accumulation at the top of the goaf.

Chan et al. [110] conducted a controlled experiment in which long-flame coal samples with particle size ~30 mm and porosity 0.3 were placed in a heating tank under a constant rate airflow of 1 Liter/min. The samples were subject to heating at eight temperature values, from 30 to 350 °C and the radon concentration exhaled from coal was measured after the thermal oxidation of coal. The dependence of radon concentration on temperature followed a pattern consistent with that described by other authors, showing a peak around 150 °C. However, unlike previous experimental studies, a second peak corresponding to coal pyrolysis was not observed. Instead, the radon concentration decreased continuously up to 350 °C. In order to gain further insight, a numerical simulation was conducted on a model presented in Figure 1 (left, the physical system and right, the mesh and the dimensions).

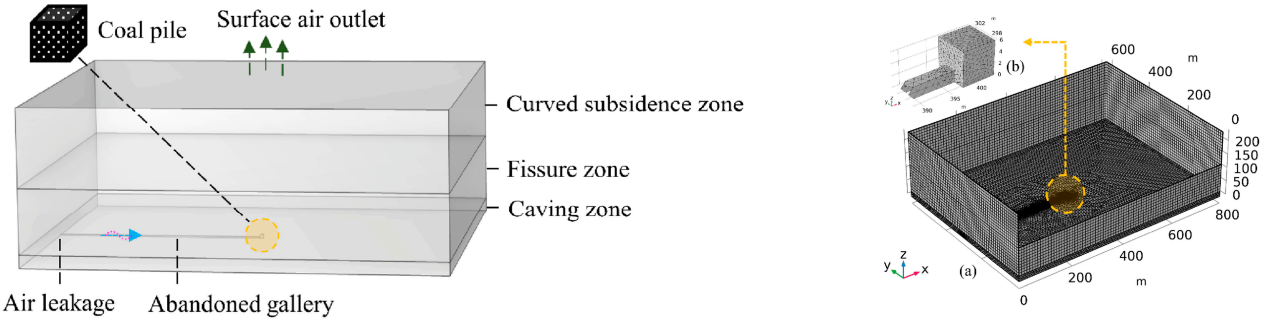

Figure 1. The physical model considered in [110] (**left**) and the mesh with dimensions (**right**): (a) overall view and (b) detail view of the coal pile. Reproduced from [110] with permission from Elsevier.

This study is interesting as it investigates an important characteristic of the geological strata, that is the air circulation inside the stock pile, as shown in Figure 2. A high value of the velocity gradient can be observed in the entrance region of the coal stockpile.

The air flow is one of the key factors that controls the CSC in the coal stockpile. In the entrance region, on the path denoted a in Figure 2-left, the air velocity has the highest values, which intensifies the convective heat transfer. As a result, high temperature regions cannot develop in this region since heat is rapidly removed. The moderate air velocity on the paths

denoted b and c and the longer trajectory compared to the path a create the conditions for the coal oxidation and heat accumulation. The radon concentration profile in the coal stockpile is presented in Figure 3. In Figure 3a the radon concentration on the sides of the stockpile is plotted after 15, 35 and 48 days. A steady increase in the radon concentration on the upper side is consistent with the field and controlled experiments reported by other authors. In the early stages of the CSC, radon accumulations occur at the base of the coal stockpile. As the CSC progresses in time, the radon concentration distribution increases in a non-uniform manner due to the effects of airflow and temperature gradients. On the windward side, the temperature is lower, leading to reduced radon emission. Additionally, the higher airflow velocity in this area facilitates the transport of radon to other locations, resulting in a lower radon concentration on the windward side of the coal pile. At the early stage of coal spontaneous combustion, the radon concentration is higher on the leeward side at the base of the coal pile due to reduced gas flow and initial oxidation reactions. However, in the later stages, the radon concentration decreases as the self-heating process in the coal is inhibited. A key conclusion from this study is that the porosity discontinuity at the interface between the caving zone and fissure zone (Figure 1) acts as an obstacle for the radon flow, resulting in a radon accumulation and a continuous increase in the concentration at this interface. This provides mass and pressure gradient to support the long-distance migration of radon, which can pass through geological structures and reach the surface. Thus, the position of the radon anomaly peak is longitudinally consistent with the position of the fire. Moreover, the peak value of the radon concentration is positively correlated to the fire source temperature.

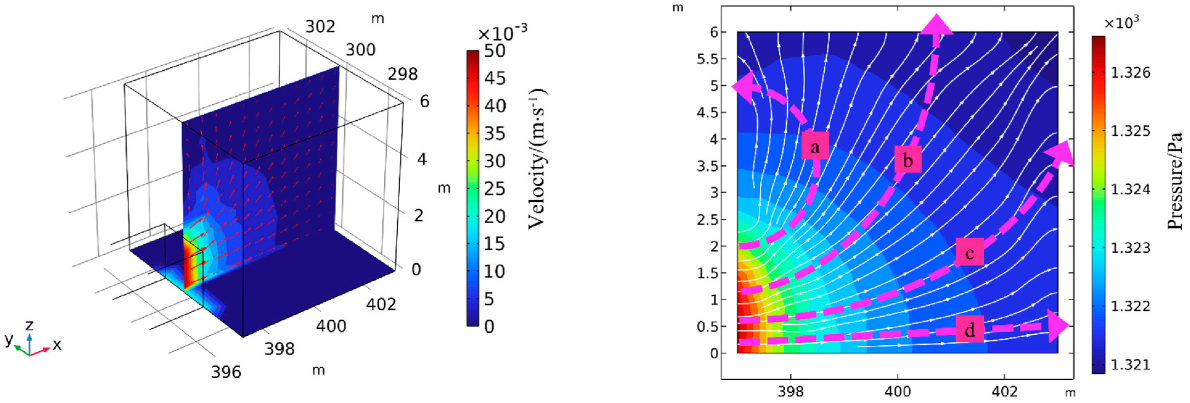

Figure 2. (**left**) Air velocity profile (and streamlines) inside the coal stockpile. (**right**) The pressure distribution and the potential lines inside the stockpile: a—high-velocity, short-length air path; b, c—moderate-velocity, long air paths; d—moderate-velocity, medium-length air path Reproduced from [110] with permission from Elsevier.

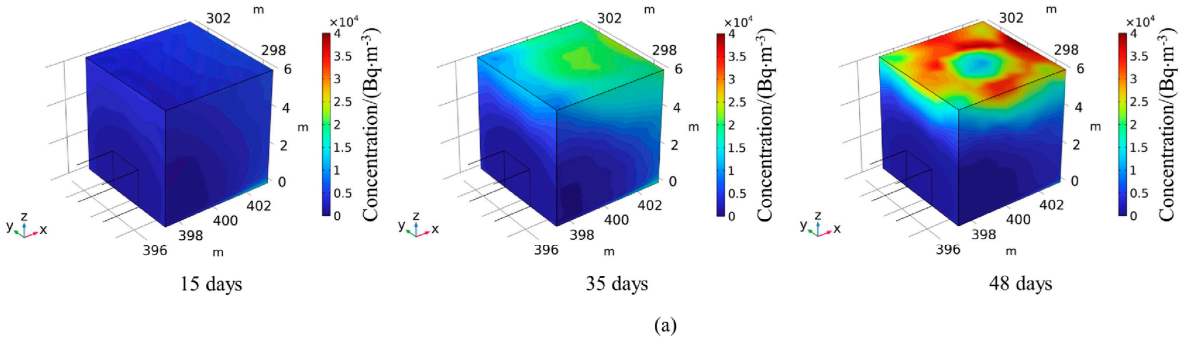

(a)

Figure 3. *Cont.*

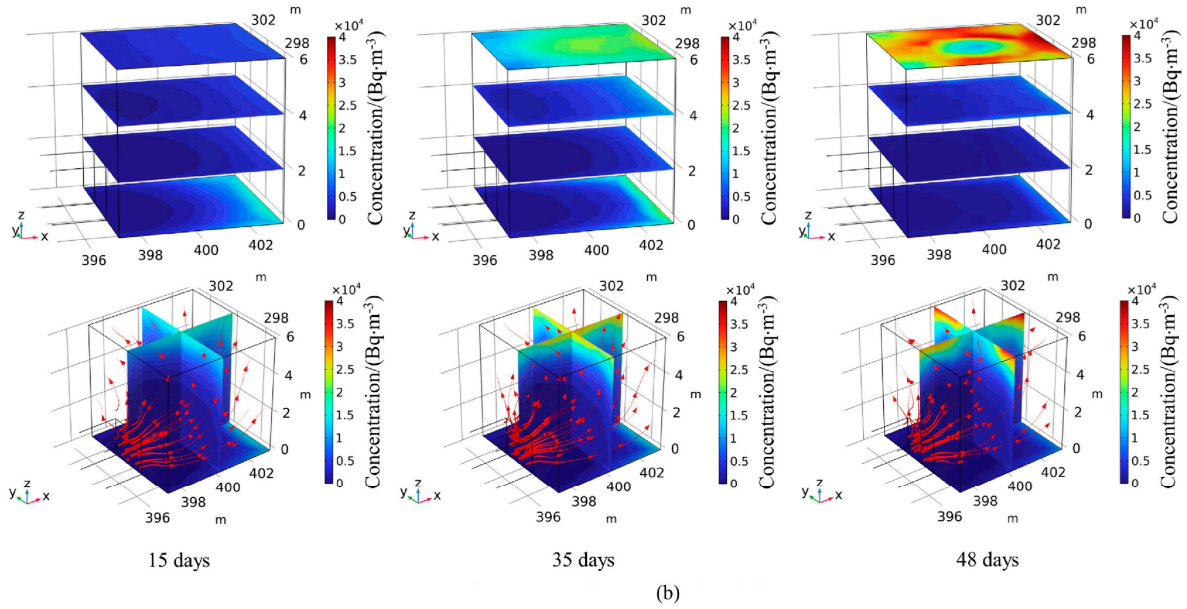

Figure 3. (**a**) The radon concentration on the faces of the coal stockpile. (**b**) The radon concentration in horizontal and vertical planes. The streamlines are depicted as red three-dimensional curves, with arrows illustrating the direction of velocity. Reproduced from [110] with permission from Elsevier.

A selection of experimental studies relating the CSC to the radon gas emission is presented in Table 4.

Table 4. Laboratory and field studies investigating the radon emission mechanisms during CSC.

Ref.	Experiment	Results
Wen et al. [111] 2020	Controlled experiment: Coal samples from the underground working face CJG (China). Coal particles with maximum size 5–7 mm. Experiments performed in a spontaneous combustion experimental furnace.	The experimental data were modeled by fitting an exponential function to the observed values. A robust correlation was identified between radon concentration and temperature within the thermal range of 50–350 °C, as evidenced by a coefficient of determination (R^2) of 0.94, indicating a strong goodness of fit. This suggests that radon emission is highly sensitive to temperature variations within this interval. However, at temperatures exceeding 350 °C, a pronounced increase in data variability was observed, likely due to complex underlying physical processes not accounted for by the exponential model. This scatter indicates a potential departure from the initial correlation, suggesting that the mechanisms governing radon release may change significantly at higher temperatures.
Du et al. [62] 2021	Field measurements: A sampling system consisting of a negative pressure air sampling pump and a sampling pipe inserted in the soil at approximately 1 m. Surface temperature measurement conducted by IR imaging on a 1600 × 450 m area known for underground coal fires. Boreholes were drilled in high surface temperature areas to measure temperature and gas concentration.	No match was observed between IR imaging high temperature regions and radon local concentration. This was attributed to factors such as • The hot gas flow generated during the CSC causes the heating of the geological structures along the air leakage path. Different physical characteristics of the geological strata cause different temperature levels. • The detection depth of radon is higher than the IR imaging. • The radon migration speed in soil is different depending on the soil permeability, being much higher in fissures and cracks than solid rock.

Table 4. *Cont.*

Ref.	Experiment	Results
Zhou et al. [108] 2021	Controlled experiment: Four coal ranks (with the corresponding Radium nuclide content in Bq/kg) were investigated: lignite (54.2), long-flame coal (44.4), coking coal (31.2) and lean coal (37.7). 1. The sealed tank was heated to 30, 50, 100, 150, 200, 250 and 300 °C. An air pump was simultaneously connected to the inlet gas pipe to oxidize the samples in the sealed tank for 48 h. 2. When the coal samples oxidation was completed at a constant temperature, the inlet and outlet gas pipes, dryer, and Rad7 radon detector were connected in a closed loop to measure the radon concentration in the tank. A total of two-hour 24 cycles was set for radon measurement at each temperature. A low-temperature nitrogen adsorption method was used to measure the specific surface area of the coal samples at different temperatures.	Radon exhalation of the coal increases rapidly with increasing oxidation temperature. The temperature corresponding to the peak radon concentration depends on the coal rank. The two-stage coal exhalation mechanism was confirmed by the radon concentration–temperature curve. Two characteristic vertices were identified on this curve: (a) The absolute maximum value, corresponding to the water evaporation temperature at approximately 100 °C. (b) The coal pyrolysis temperature, corresponding to the second stage of the exhalation process, occurring at approximately 250 °C. The specific surface area (m^2/g) first decreases with the temperature reaching a minimum value at roughly 200 °C and then it increases abruptly after 250 °C as the coal undergoes the pyrolysis process. The downward trend in specific surface area up to 200 °C suggests that it is not the primary factor contributing to the increase in radon concentration.
Zhou et al. [68] 2018	Field measurements conducted on the gob of a small abandoned coal mine in the region Bao Shan Yao Zhai (China). Radon concentration in the soil was determined by means of an alpha-cup emanometer (Ding et al. [112]). The procedure consisted of burying the frustum-shaped alpha cup for 4 h at 30–40 cm. Two measurement fields were defined: field I with an area of 396,000 m^2 and field II with an area of 89,600 m^2. The basic point distance was 20 × 20 m with a total of 1530 measurement points: 1050 in field I and 480 in field II.	A 2D color map of the radon concentration was created, showing the coordinates of the high concentration areas. Drilling verification was performed in the radon high value zone of area A confirming an abnormal temperature area.
Hu et al. [113] 2023	Controlled experiment with long-flame coal disk-shaped (Φ50 × 20 mm) samples collected from Yunlin region (China) heated at 5 °C/min up to the set point and then maintained for 1h. Two sets of experiments were conducted, aerobic and anaerobic (with samples wrapped and sealed to prevent oxygen exposure). The radon emission concentration after cooling down to the ambient temperature was measured.	Temperatures values of 300 °C and 500 °C are pivotal in altering the properties the investigated coal. At these values, there is a significant increase in the mass loss ratio, specific surface area, pore volume, and fracture ratio. The expansion and propagation of pores and fractures, along with the release of substantial amounts of pyrolysis gases, result in a massive desorption and dispersion of radon. The radon release rate from pyrolysis products is inversely correlated with specific surface area, pore volume, and fracture ratio. The development of fissures and the reduction in radon emission rates are more pronounced in the aerobic environments. Elevated temperatures promote the transformation of dissolved, adsorbed, and trapped radon into free radon within the coal, thereby accelerating its migration rate. This results in a decrease in the residual radon content in pyrolysis products and a marked reduction in the radon exhalation rate. There is a negative correlation between the heating temperature and the radon emission rate.

3.1.3. Gas Emission Assessment—Insights and Unexplored Areas

The gas analysis with the purpose of detecting the CSC in various phases is a feasible approach considering the relative simplicity and cost effectiveness of the technique. The gas sensor systems commercially available are precise enough and the measurement chains are in general fast and accurate. Rugged, fault-tolerant gas measurement systems were designed for the harsh mining environment. These systems are in general more expensive and they still require periodic calibration and verification, as they are critical sensor applications. For such applications, parameters such as precision (the number of true positives divided by the total number of positive predictions) and recall (the number of true positives flagged by the system divided by the total number of fire incidents) are of extreme importance.

No relevant studies on these important issues were identified, although there are many incident reports where gas emission-based CSC detection techniques failed to detect the fire [93].

The usual gas monitoring systems are discussed comparatively from the advantages/disadvantages point of view in Table 5.

Table 5. Gas monitoring techniques currently integrated in CSC detection systems.

Gas Monitoring Technique	Advantages	Disadvantages
Gas analyzers located at the surface with a tube bundle system. Consist of PET tubes extended from the surface to selected locations underground. The tubes are general high-grade quality non permeable materials with a variable diameter ranging from 6 mm to 20 mm (depending on the length) and lengths of up to several km. Negative pressure pumps located on the surface ensure the gas circulation.	With integration of flame traps, no explosion-proof devices are required. Most of the primary components are positioned on the surface, which simplifies maintenance. Calibration of the analyzers can be conducted on the surface. No power required for underground components. Analyzers available for a wide range of gases.	Leakage and infiltrations in the tube system cannot be easily identified. Results are not in real time. Moisture removal systems failure results in formation of liquid droplets, which hinder the gas circulation or cause erroneous readings. Tubes may be easily damaged by fire, explosion or earth works.
Real-time telemetry systems. Consist of fixed sensors are generally installed where real-time data are required. Sensors suitable for this type of systems: catalytic combustion (CH_4), electrochemical (CO and O_2), and IR detectors (CO and CH_4).	Real-time indication Since gas sensors generate an electrical signal, they can be positioned at significant distances from the analyzer. A sensor failure cannot go unnoticed.	High maintenance. Limited sensor life. Not suitable for oxygen deficient atmosphere. Some sensors exhibit cross sensitivity. Catalytic sensors may undergo poisoning.
Periodic inspection using portable devices.	Diversity and flexibility in selection the sampling location. Detection accuracy depends on the accuracy of the analyzer device.	Not possible to use behind sealed boreholes or closed seams. Continuous monitoring not possible. Personnel cost.
Sampling using gas bags subsequently analyzed by a gas analysis service provider.	High precision. A wide range of gases can be detected.	Results are not in real time. Expensive. Not possible to use behind sealed boreholes or closed seams. Continuous monitoring not possible. Personnel cost.
Gas chromatographic systems. Ultra-fast micro gas chromatographs.	A wide range of gases can be detected. Fast analysis (in minutes). Simple to operate. The ability to detect and analyze key components of spontaneous combustion, such as H_2, CO, ethylene, ethane, and propylene, at concentrations ranging from parts per million (ppm) to percent levels. This requires a single type of detector, specifically a thermal conductivity detector for analyzing the mine atmosphere.	Expensive. High maintenance.

Accurate and timely detection of CSC in its early stages using index gas methods presents a complex challenge that extends beyond sensor accuracy. A significant influence is exerted by the specific conditions and characteristics of the mining facility (such as coal gob or coal seam) and the properties of the coal itself. Modifications in the local atmosphere (e.g., CO and CO_2 emissions from thermal engines, CO_2 absorption in water, CO consumption due to bacterial activity) and transient environmental conditions can cause interferences, leading to deviations in sensor measurements from actual conditions. While CO can serve

as a reliable indicator of CSC initiation under controlled laboratory conditions, in real-world industrial settings, numerous and unpredictable interferences render CO-based CSC detection systems unreliable. To address this issue, the concept of composite index gases was introduced, as outlined in Table 2. However, composite indices may also be subject to similar limitations as single gas indices due to their dependence on gas sensors. Although composite indices may offer greater robustness in detecting CSC under certain conditions compared to single gas indices, their effectiveness remains influenced by the coal rank and the specific conditions of the mining environment, Gbadamosi et al. [114].

Radon gas detection methods rely on the exhalation of radon driven by temperature increases. Due to the strong correlation between radon exhalation rates and temperature, these methods exhibit robustness and are relatively less affected by specific mining factors. However, the coal rank significantly influences both the exhalation rate profile and the observed local maxima. A critical challenge for radon-based methods lies in the radon migration from subsurface to surface levels. The local geological morphology, characteristics of geological formations, and the presence of fractures and fissures can lead to substantial deviations between the surface detection points of peak radon concentration and the actual underground locations of CSC development. Another notable limitation of radon-based methods, in comparison to index gas methods, is their inability to be integrated into real-time measurement systems. Consequently, these methods do not provide instantaneous detection.

Most of the experimental studies identified and included in this review are conducted in controlled laboratory conditions, which might limit the generality of the conclusions.

3.2. Electromagnetic, Acoustic and Optic Techniques

3.2.1. Electromagnetic Effects

Coal heating resulting from low-temperature oxidation and combustion induces modifications in the surrounding magnetic and electric fields (de Boer et al. [115]). The generation of electromagnetic radiation (EMR) signals in response to coal heating is a well-established phenomenon (Kong et al. [116], 2018), though the underlying mechanisms are complex and not yet fully elucidated. The sources of EMR charges during coal deformation and fracturing include (Wang et al. [117]): (1) transients of electric dipoles (electric dipole layers) induced by applied stress, (2) variable motion of separated charges due to crack propagation and frictional interactions, (3) energy dissipation associated with oscillations in RC circuits within fractured coal walls, and (4) relaxation of separated charges coupled with electromagnetic radiation resulting from high-velocity particle collisions with wall cracks.

The volumetric thermal expansion induced by heating leads to deformation and detachment of the morphological structures within the coal matrix. As temperature rises, the thermal swelling stress within the coal increases proportionally, thereby enhancing the likelihood of coal deformation and fracturing. Upon reaching a critical temperature, the tensile strain experienced by the particles within the coal exceeds their ultimate tensile strength, resulting in the disruption of mineral particle interfaces. This process generates microcracks and facilitates the propagation of slip within the coal structure. (Kong et al. [118], 2016). The non-uniform thermal expansion and deformation of particles within the coal matrix induces the migration of free charges from regions of high concentration to regions of lower concentration. This differential expansion creates various stress and density zones within the coal. Consequently, charge clusters with varying densities accumulate in these distinct stress and density regions, leading to the formation of numerous dipoles, which subsequently emit electromagnetic waves (Kong et al. [119], 2017). During the processes of coal deformation and failure, non-uniform strain induced by charge transfer, piezoelectric effects, frictional interactions, chemical bond rupture, and dislocation slip under thermal stress can result in charge separation. When the internal stress in the coal exceeds the critical stress threshold for crack initiation, cracks develop and propagate. This process generates free electrons that were previously bound at the crack tips, converting them into

free electrons. The movement of these free electrons generates EMR signals due to their displacement and interaction with the surrounding field (Kong et al. [120], 2018).

Electric properties of coal play a pivotal role in the characteristics of the EMR signal generated during the coal heating. Zhu et al. [121] investigated in a laboratory-controlled study the dielectric spectrum of coal during oxidation, reporting that the dielectric constant initially decreased up to 150 °C due to reduced dipole polarizability from moisture release, then it increased between 150 °C and 275 °C. Up to 225 °C, the increase was attributed to the formation of oxygen-containing bonds outpacing their breakage, enhancing dipole polarization. Beyond 225 °C, changes in oxygen bond quantity and molecular chain deformation were the main causes of the increase. The dielectric constant then dropped sharply until 400 °C which was attributed to the rupture of polar bonds and volatile release, before increasing again beyond 400 °C, likely from enhanced electron migration.

The variation in the coal electrical resistivity with the temperature was investigated in a laboratory-controlled experiment by Zhu et al. [122]. Coal samples from five different mining regions were considered. Coal from two of these regions was known for having a high spontaneous combustion tendency while coal from one region was known to be stable to low-temperature oxidation. An impedance analyzer was employed to determine the real and imaginary parts of the impedance. Under an alternating current ranging from 20 Hz to several MHz, the volume resistivity of coal samples exhibited a consistent pattern with frequency: it decreased rapidly at mid to low frequencies and more gradually at mid to high frequencies. At a test frequency of 100 kHz, the resistivity initially increased with temperature and then decreased. At the same frequency, both the real and imaginary components of the coal's complex relative permittivity decreased with increasing temperature, with a progressively lower slope. Due to the segmented variation in the resistivity-temperature relationship, the same resistivity value can correspond to multiple temperatures. As a result, resistivity alone cannot accurately determine the coal's temperature, and the imaginary part of the complex permittivity shows a similar limitation. Therefore, when using resistivity to infer the temperature in a fire zone, the geological conditions and other characteristic parameters must be considered for accurate interpretation.

In a laboratory-controlled experiment, Kong et al. [116] (2018) measured the variations in the EMR field produced during the low-temperature oxidation and combustion of coal. During the spontaneous combustion of coal, distinct electromagnetic radiation (EMR) signals are observed, with their intensity increasing in direct correlation with rising temperatures. The EMR signals measured at frequencies of 100 kHz and 1 MHz demonstrate nearly identical variation patterns, indicating a consistent response across different frequency ranges. Quantitatively, the EMR signals exhibit a positive correlation with temperature, characterized by a correlation coefficient greater than 0.73, suggesting a strong linear relationship. Moreover, the EMR signal intensity showed a substantial correlation with the evolution of CO volume, reflecting a parallel change trend that underscores the potential of EMR monitoring in tracking combustion progression and gas release dynamics. An experimental field study conducted by Kong et al. [72] (2019) attempted to correlate the EMR spectrum with the CSC in a section of a mining area where IR imaging revealed several hot-spots (~55 °C). The underground temperature measurements showed an ongoing spontaneous combustion process, with temperatures exceeding 300 °C. The correlation between the heatmap and the EMR spectrum is presented in Figure 4 using the data obtained by applying the Kriging interpolation method to compute the variogram of the EMR data collected from 20 measuring points across 5 measurement lines within the high-temperature region.

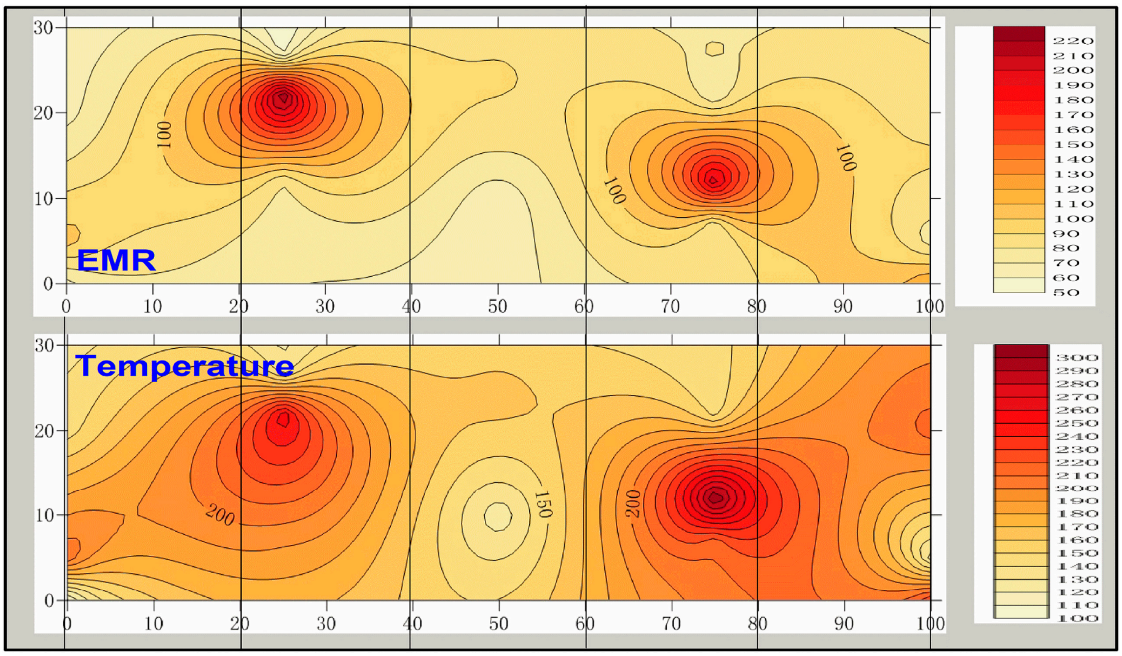

Figure 4. EMR spectrum and surface heat map. Reproduced from [72] with permission from Elsevier.

3.2.2. Electric Properties

Karaoulis et al. [123] proposed a combined method consisting of simultaneous inversion of self-potential and resistivity data, employing joint attribute analysis to delineate and localize the burning front of a coal seam fire. The experimental study was applied to a subbituminous coal formation fire at depth value ranging from 10 to 15 m. The self-potential survey systems comprised 160 measurement stations distributed across 5 profiles, with 32 stations per profile, positioned at the ground surface. The observed self-potential anomalies ranged from +70 m to −50 mV relative to a reference point located distal to the burning front. The resistivity survey included 5 profiles, each with 118 measurements, totaling 590 resistivity readings. The burning front was characterized by extremely low electrical resistivity values (<15Ω • m) and a source current density likely attributable to thermoelectric effects. The integrated inversion and interpretation of self-potential and resistivity data distinctly delineated the position of the coal seam fire. This finding was further validated by the detection of a thermal anomaly at a depth of 30 cm and observation of sporadic hot steam, suggesting a minimum depth for the thermal source of approximately 9 m. The high-resolution earth resistivity method, initially developed to detect underground cavities (bunkers, tunnels, etc.) was applied to detect underground burning areas by Shi and Wu [124]. The method consists of placing the potential electrode at one end of the survey line. A current is injected into the ground through a series of current electrodes, and the corresponding potential differences are measured at the initial position of the potential electrode. The potential electrode is then moved to the next measurement point along the survey line, and the process is repeated: current is supplied sequentially through each current electrode, and the resulting potential differences are recorded. This procedure continues until the potential electrode reaches the opposite end of the survey line. By following this sequence, a complete two-dimensional profile of electrical potential differences along the survey line is obtained. Uneven electrical properties of the Earth's surface may cause serious errors for this method. The second method described in Shi and Wu [124], which overcomes the main drawback of the high-resolution earth resistivity method, is the transient electromagnetic method. An ungrounded loop or grounded line source is used to send a primary electromagnetic pulse of a specific waveform into the ground. Between these pulses, a coil or grounded electrode is used to measure the secondary magnetic field (caused by eddy currents) or the space-time distribution of the induced electric field. This method provides information about the electrical properties of

underground geological structures. Compared to the frequency-domain method, the transient electromagnetic method offers higher detection accuracy, as measurements are taken from the same location, reducing issues related to recording points. Additionally, the use of a loop device minimizes the effects of static shifts caused by surface electrical property variations and is less affected by terrain changes. Therefore, this method is particularly suitable for detecting burned areas and high-temperature centers in combustion zones, making it a critical component of the comprehensive electromagnetic approach discussed in this study. The results of the two methods are presented in Figure 5 (left, high-resolution earth resistivity and right, transient electromagnetic method).

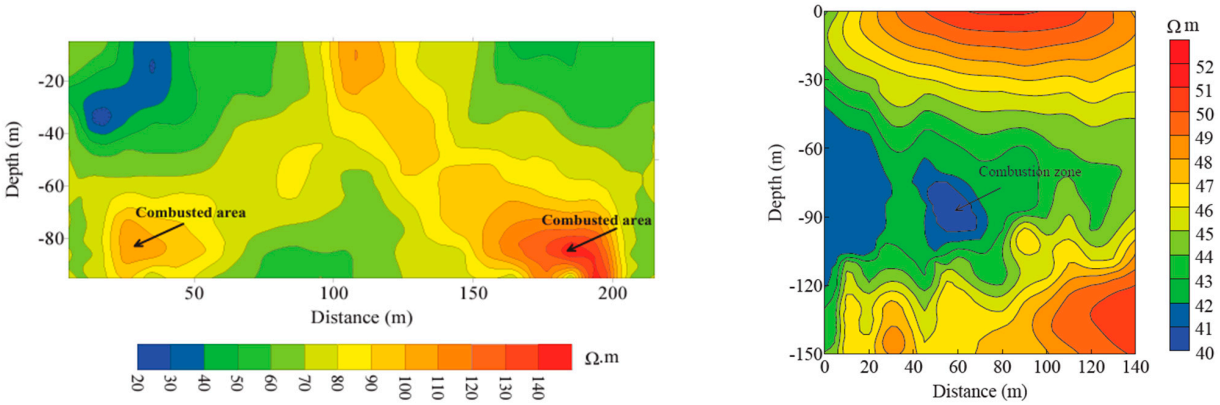

Figure 5. Apparent resistivity profile determined through the high– resolution earth resistivity method (**left**) and transient electromagnetic method (**right**). Reproduced from [124] with permission from Elsevier.

The modification of the acoustic properties of solids with temperature is another method that allow for identification of areas where CSC exists. Two methods that rely on temperature-induced modification of the acoustic properties exist: (i) methods that are based on the change in speed of sound and (ii) methods that determine the change in frequency of the acoustic wave. Acoustic velocity thermometry is a commonly employed technique for measuring temperature. This method involves determining the propagation velocity of an acoustic wave by measuring its travel time over a known distance within the medium of interest. The temperature of the medium is then inferred from the established relationship between acoustic wave velocity and temperature. The sound source signals used in acoustic thermometry typically encompass both low- and medium-frequency acoustic waves, as well as ultrasound. Ren et al. [125] conducted acoustic attenuation tests in an experimental study in a laboratory-controlled environment with four types of coal (lean coal, coking coal, non-stick coal and long flame coal) prepared into seven particle size distribution ranges (>10 mm, 7–10 mm, 5–7 mm, 3–5 mm, 0.9–3 mm and <0.9 mm). An experimental apparatus consisting of an impedance tube, acoustic driver (loudspeaker), microphone array, and data acquisition system was employed to quantify the attenuation coefficient over a specified range of frequencies and temperatures. For all coal samples and temperature conditions, the attenuation coefficient demonstrated a non-linear, oscillatory behavior with local maxima superimposed upon a generally increasing trend. A modest increase in the attenuation coefficient was observed with rising temperatures. Attenuation peaks were detected at frequencies of 400, 700, 1100, and 1600 Hz, which can be attributed to mechanisms of acoustic absorption and scattering resulting from the granular and porous nature of the coal. Deng et al. [126] used a similar experimental setup to investigate the acoustic attenuation characteristics of anthracite, using coal samples collected from Si he coal mine (China). Pseudo-random, pulse, and swept-frequency acoustic signals were utilized in this study to evaluate the attenuation characteristics of anthracite coal. The findings indicated that the pseudo-random signal exhibited the highest attenuation, whereas the pulse signal demonstrated the greatest sensitivity to temperature variations.

When estimating the temperature of anthracite coal using an optimized acoustic signal composed of a linear frequency sweep between 600 and 1000 Hz with a 0.1 s duration, the maximum absolute temperature error was determined to be 4.22%. In a laboratory-controlled study, Kong et al. [127] (2024) built a test system for exploring the sound wave kinematics parameters in the process of CSC. The elastic wave computed tomography (CT) inversion algorithm was employed to reconstruct the acoustic wave velocity field, which was subsequently used to infer the temperature distribution within the coal sample. Results indicated that regions of elevated sound wave velocity corresponded to areas exhibiting temperature anomalies, particularly in zones with higher coal temperatures. The accuracy of the reconstructed sound velocity field was validated through correlation with the results obtained from single-path acoustic velocity measurements. This study also proposes a hypothesis to account for the variability of sound velocity in regions affected by CSC. Scanning electron microscopy (SEM) analysis revealed that as the temperature rises, the extent of damage and fracturing of coal particles increases, resulting in the expansion of inter-particle gaps. As sound waves propagate through these gaps, the elevated air temperature within them contributes to an increase in sound velocity. Consequently, the velocity of sound waves rises in tandem with the heating of loose coal.

Liu et al. [128] developed a laboratory-scale experimental setup to investigate infrasound signals generated during the CSC process. Their study aimed to establish the frequency domain characteristics and the correlation between infrasound signals and CSC temperature. The analysis focused on the frequency domain and energy characteristics of infrasound waves across different stages of the CSC process. Two key conclusions were derived from this study: (i) The time-domain analysis revealed that the infrasound waves generated during CSC can be classified into three distinct stages: a stable stage, a development stage, and a rapid increase stage. The infrasound signals exhibit intermittent characteristics, with the primary frequency amplitude of these waves showing a strong correlation with temperature, evidenced by a correlation coefficient exceeding a certain threshold. (ii) The energy of infrasound waves is predominantly concentrated in the low-frequency range of 0–0.12 Hz during the process of CSC. The distribution of infrasound energy across different frequency bands varies significantly at different stages of CSC. As temperature increases, the proportion of energy within the 0.04–0.08 Hz frequency range progressively rises, while the energy proportion in the 0–0.04 Hz range diminishes. The observed increase in infrasound energy within the 0.04–0.08 Hz band serves as a critical precursor to the onset of CSC.

A comprehensive review on the application of complex acoustic wave techniques was conducted by Guo et al. [66]. All studies included and discussed in this review were conducted in laboratory-controlled environments. The majority of the studies converge in several key findings: (i) Combustion-generated sounds and externally applied acoustic signals can interact to create a dual-source composite acoustic wave. However, the effects of superposition and mutual interference between these source waves on the waveform and characteristics of the composite wave remain poorly understood. The application of dual-source acoustic thermometry is constrained by challenges in separating the composite wave spectrum and comprehending the influences of coal properties and gas composition on these interactions. (ii) The acoustic emissions generated by the spontaneous combustion of loose coal in mining areas are significantly influenced by several factors, including the degree of coal metamorphism, coal temperature, void characteristics, and surrounding gas conditions. Developing a relationship model that correlates these factors with acoustic signals will likely be a key advancement in the field of acoustic temperature measurement of coal.

3.2.3. CSC Detection Based on Magnetic Effects

Magnetometry surveys are effective in detecting underground anomalies induced by coal spontaneous combustion (CSC) due to changes in magnetic susceptibility resulting from thermal alteration of the medium. In a magnetometry survey conducted by Ide

et al. [129] in the San Juan Basin, USA, the magnetic susceptibility of thermally altered overburden samples at the NCF was measured using a kappa bridge system. The study revealed that these altered samples exhibited magnetic susceptibilities significantly higher than the natural, unaltered values, by one to two orders of magnitude. Diurnal variations in the Earth's magnetic field and anomalies caused by metal objects were mitigated through filtering techniques. The results demonstrated high repeatability and enabled monitoring of the advancement of the combustion front. However, a notable limitation of this method is that geological structures affected by subsurface fires often contain substantial concentrations of magnetite, which can influence the accuracy of the measurements. Shao et al. [130] conducted a comprehensive field study on the Heshituoluogai coal fire in China, which encompasses 12 sub-fire areas across 57 km^2, totaling 1,444,220 m^2. Magnetic and self-potential anomaly data were collected using a magnetometer and an intensification-polarization instrument. Laboratory experiments revealed that rocks overlying a subsurface fire, when heated beyond the Curie temperature, exhibit significant changes in magnetic properties, such as magnetic susceptibility and thermoremanent magnetization. Data processing techniques, including diurnal fluctuation rectification, reduction to pole, and upward continuation, facilitated clearer interpretation of the results. The fire locations identified through magnetic and self-potential methods aligned with ground survey findings, demonstrating the effectiveness of these techniques for detecting coal fires. Additionally, the study found that the redox and Thomson potentials, resulting from coal combustion at high temperatures, induce self-potential anomalies: positive anomalies indicate shallow fires, while negative anomalies suggest deeper fires (beyond approximately 30 m).

3.2.4. Summary and Future Perspectives

Electromagnetic/electric, magnetic, and acoustic measurement techniques offer several advantages over gas-based detection methods. These techniques provide extensive spatial coverage beyond the immediate vicinity of the sensor, involve relatively low installation and maintenance costs, and are adaptable for detecting fires in underground coal seams, stockpiles, and coal silos. Despite a significant body of research on electromagnetic/electric-based detection of spontaneous coal combustion (CSC), several limitations affect their applicability. Challenges include the complexity of electrical phenomena, the variability in the electromagnetic properties of coal and geological structures, and the inconsistency of site conditions. While some studies (e.g., Kong et al. [127]) have successfully characterized subsurface fires using electromagnetic effects, further research is needed to generalize these findings across different sites, coal ranks, and geological morphologies. The mechanical–electrical and thermoelectrical coupling models depend on various mechanical, electrical, and thermophysical parameters that differ to a significant extent among coal ranks and geological formations.

Magnetometry has two principal limitations: (i) magnetic anomalies detectable by this method occur only at high temperatures, indicating that CSC is already fully developed, and (ii) the geological structures above the coal seams must contain a sufficient amount of magnetite. Furthermore, magnetic anomalies are highly sensitive to the magnetic concentration, which varies from site to site.

Acoustic techniques also present potential for CSC detection, with advanced systems capable of accurately locating the combustion front. However, these technologies are still under development and face significant challenges. Issues include the complex and heterogeneous nature of the propagation medium—comprising coal matrices with varying morphologies and gas- or air-filled voids—which affects acoustic wave propagation in ways that are not yet fully understood or consistently reproducible. Additionally, the technology has not yet achieved the maturity required for standardization and widespread use.

4. Surface and Combined Techniques

Surface techniques are mainly based on the temperature measurements, in general, by IR thermography. Surface techniques have several major advantages in comparison to

underground techniques: (i) no physical contact is required; (ii) real-time heatmaps can be produced; (iii) with little effort, large surface areas can be monitored. However, it has to be noted that the surface heatmap does not always offer an accurate image of the CSC progression developing underground, and a set of hard-to-control factors can interfere with the quantitative measurements of surface techniques: subsurface geological structures morphology and dimensions; environmental factors (ambient temperature and humidity, wind speed and direction, solar radiation intensity), and radiative properties of the surface (emissivity and albedo).

Field studies attempting to characterize the CSC by means of IR thermography were reported by Pandey et al. [131], Misz-Kennan and Tabor [132], and Roy et al. [133]. Hu et al. [71] conducted an empirical investigation at a decommissioned coal waste dump in Changping, China. The experimental site was configured as a conical heap with a base diameter of 2.5 m and a height of 1.8 m, totaling approximately 2767 kg in mass. The coal waste comprised subbituminous coal, sandstone, clay, quartzite, sulfide mineralization, and various solid residues. Field surveys identified potential high-temperature zones on the surface of the dump and noted a significant absence of vegetation. The methodology developed in this study encompassed four key phases: field investigation, data pre-processing, data integration, and 3D visualization. The resulting 3D temperature distribution model enabled the classification of observed zones into three distinct categories based on varying temperature levels. Gao et al. [67] employed a ground penetrating radar operating at 900 MHz in a laboratory-controlled experiment to create underground images, which were further processed by means of deep learning to identify the position and size of an underground burning area. Based on the similarity theory, a scale model was built for a coal fire developing in a coal seam with the thickness of 4.3 m at the depth of 26.9 m.

The evolution ofCSC and the corresponding ground-penetrating radar (GPR) images are depicted in Figure 6. Due to the significant difference in dielectric constants between air and rock strata, where air exhibits a considerably lower dielectric constant, the incident electromagnetic waves generate a strong reflection at the air–rock boundary. This phenomenon is characterized by a distinct hyperbolic reflection pattern in the radar images. In contrast, coal has a dielectric constant slightly lower than that of the surrounding rock, and the medium demonstrates a relatively uniform composition. This results in a clear, linear reflection interface between the coal and the adjacent rock strata. During the early stages of combustion, the amount of ash produced is minimal, resulting in a continuous signal between the combustion cavity and the coal seam in the radar image, as illustrated in Figure 6a. By comparing the radar images obtained during testing with those produced by GPR, it becomes possible to identify and interpret waveform signals indicative of coal fires. Key spatial features associated with areas of coal combustion include the combustion cavity, the active combustion front, and the subsurface collapse zones—all of which serve as primary detection targets for GPR surveys. The combustion cavity is identified by a hyperbolic reflection response accompanied by fractures that form between the hyperbolic waveforms and linear interfaces. Meanwhile, the subsurface collapse surface due to combustion is represented by a continuous, curved waveform, characterized by irregular reflection signals emanating from below the collapsed zone.

Wang et al. (2020) [134] introduced an integrated approach for delineating coal fire zones, utilizing a multi-index data fusion method that combines temperature, gas, and radon concentration measurements. The methodology incorporates non-dimensional normalization to standardize different data types and applies weight analysis using the Analytic Hierarchy Process (AHP) to assess the relative importance of each parameter. The approach employs radon gas measurements, borehole temperature data, and gas concentration measurements to create a comprehensive index of fire zone delineation (IFZD). This IFZD, derived from the fusion of multi-dimensional data, provides a robust framework for accurately identifying and characterizing the extent of underground coal fire zones. Using fractal theory, the threshold for anomalies in the Index of Fire Zone Delineation (IFZD) was established through a piecewise linear regression in double-logarithmic coordinates. This

process resulted in the development of a comprehensive multi-dimensional data fusion method for detecting underground fires, which was subsequently applied to a shallow coal seam fire in a typical integrated mining site. The analysis revealed that the weight coefficients assigned to various detection indices, namely carbon monoxide (CO), carbon dioxide (CO_2), sulfur dioxide (SO_2), temperature, and radon, were 0.12, 0.03, 0.05, 0.12, and 0.68, respectively. The lower boundary for IFZD anomalies was identified as 0.29. Utilizing the IFZD values and the corresponding anomaly thresholds, a detailed composite contour map was created, along with a plan view and a three-dimensional model of the anomalous zones. This mapping identified eight distinct areas, covering a total surface area of 27,061 square meters, with the anomalous regions extending from the vicinity of a decommissioned shaft and the main well toward the southwest and northeast. Notably, the densest contours and the highest values were found around the locations of the abandoned air shaft and main shaft, indicating severe coal oxidation in these areas. These findings underscore the need for intensified monitoring, particularly focusing on the inspection and sealing of ground fractures.

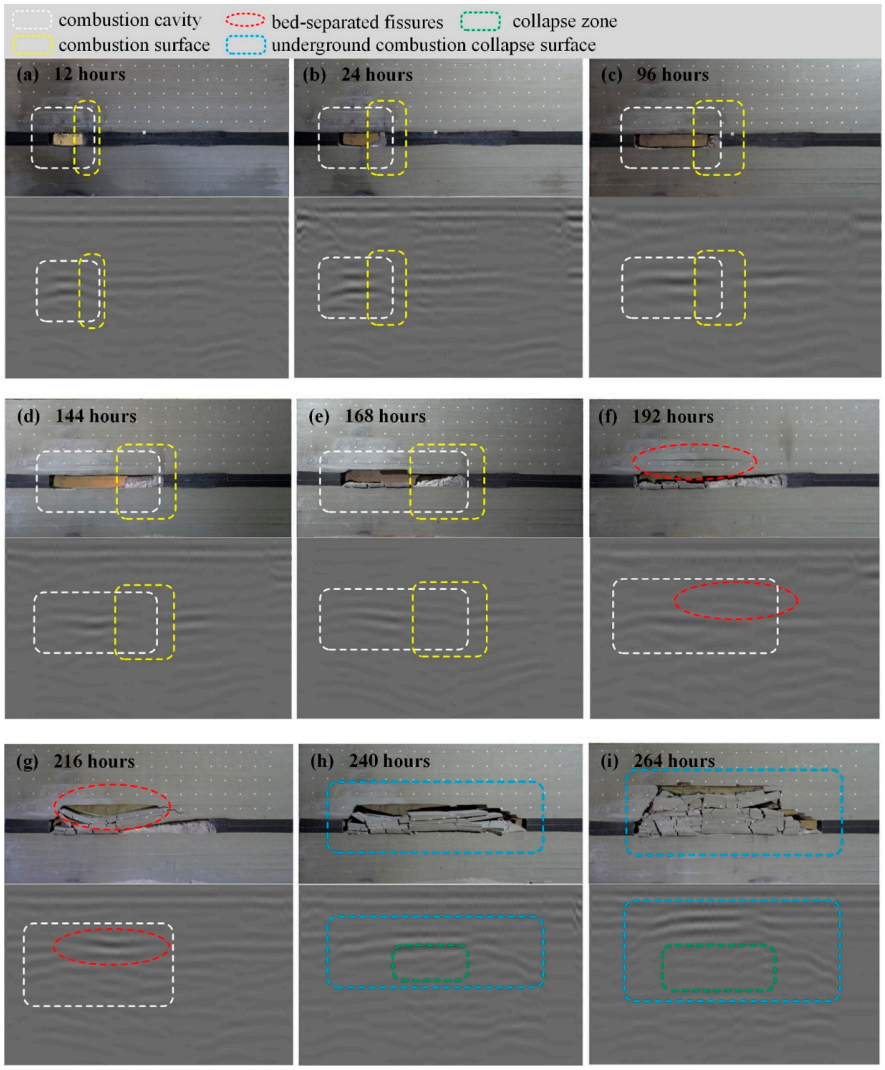

Figure 6. The advance of the simulated CSC and the corresponding radar images: (**a**) the initial stages revealed the combustion cavity in the form of a hyperbola in the radar image; (**b**–**d**) misalignment and fractures between the hyperbolic reflection and the linear interface occur due to ash formation; (**e**,**f**) thermal stress and gravity caused the roof collapse; (**g**) fissures in the adjacent strata; (**h**,**i**) collapse of the adjacent strata. Reproduced from [67] with permission from Elsevier.

A novel data-driven approach was proposed by Wang et al. (2024) [135] and applied to a coalfield in Xianjiang (China) in four characteristic regions, as depicted in Figure 7. By utilizing the atypical properties of shallow soil and surface strata as diagnostic indicators, a comprehensive evaluation framework is introduced to detect the incipient stages of combustion in coal fire areas through a data-centric methodology. A hierarchical assessment model is established for the early detection of combustion, integrating both terrestrial and atmospheric parameters. The combustion intensity at each survey point is determined by leveraging survey datasets to assign weighting factors to the assessment indicators. Geographic Information System (GIS) technology is applied to delineate the spatial distribution and boundary extents of varying combustion intensities within the surveyed region. The proposed assessment framework is validated using radon concentration measurements and infrared thermographic imaging techniques.

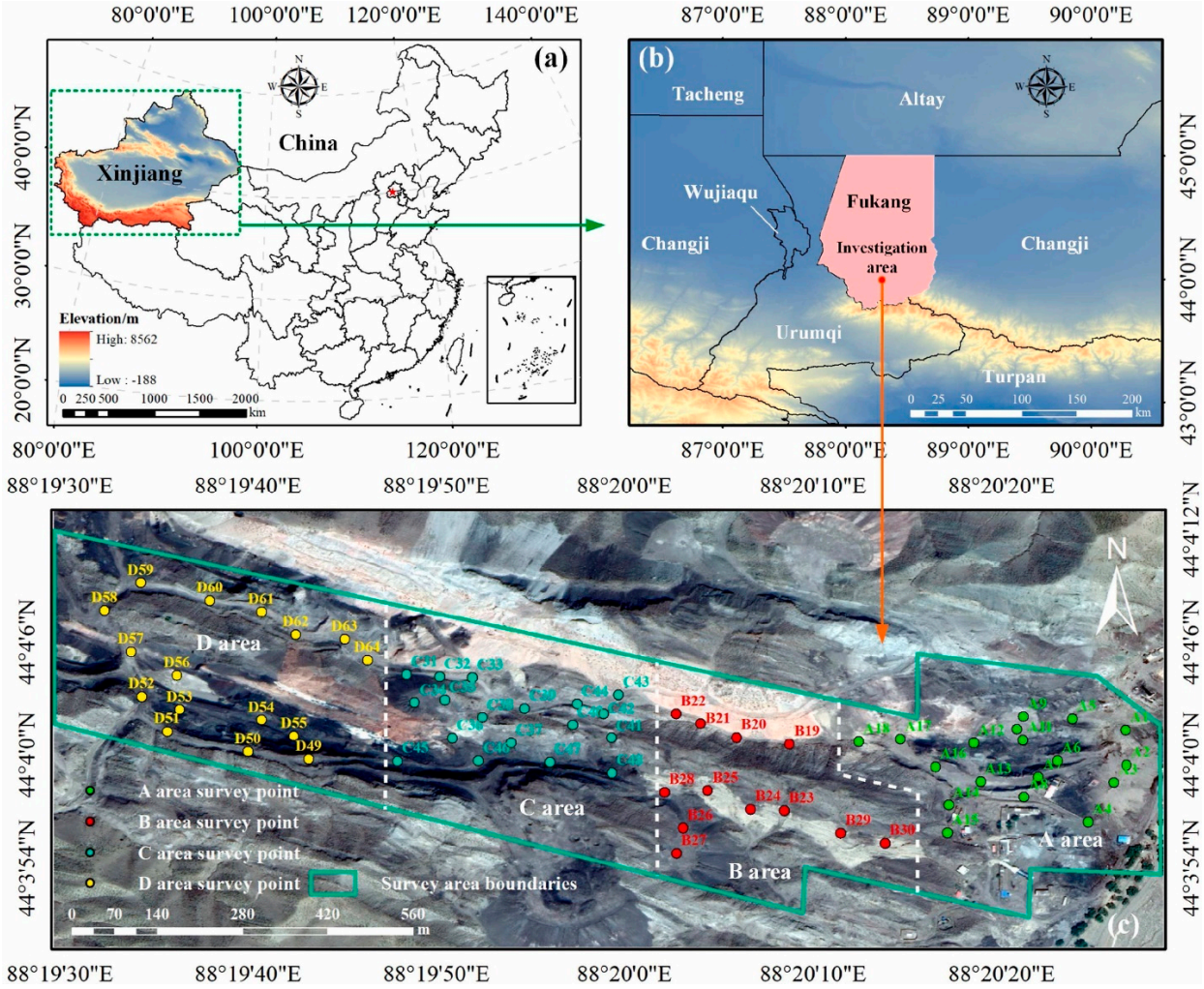

Figure 7. The coalfield where the data−driven approach presented in [135] was applied. (**a**) Map of the region Xinjiang; (**b**) Location of the survey area; (**c**) Survey boundaries and distribution points. Reproduced from [135] with permission from Elsevier.

To verify the precision of the assessment outcomes, field validation was carried out using radon gas detection and geological surveying techniques, as illustrated in Figure 8. Infrared thermal imaging was employed to examine the geological characteristics associated with risk assessment level IV, as shown in Figure 8a–d. In regions A, B, and C, where the risk level was classified as IV, surface temperatures were found to exceed 100 °C, revealing significant thermal anomalies. In contrast, no such high-temperature anomalies were detected in region D. This suggests that areas categorized under risk assessment level

IV exhibit more pronounced coal fire activity, consistent with the thermal irregularities typical of active combustion phases. The four regions (A, B, C, and D) display distinct spatial distributions of assessed risk levels. In regions A, B, and C, (locations evaluated at risk level IV) geological features such as fractures, subsidence pits, vents, and radon gas anomalies were reported. Notably, the maximum radon gas concentrations in these areas were 2672 Bq·m^{-3}, 2890 Bq·m^{-3}, and 3000 Bq·m^{-3}, respectively. This indicates that sites identified with assessment risk level IV correspond to periods of intensified coal fire combustion.

Rúa et al. [136] conducted field measurements on 23 parameters (coal seam specific as well as environmental) in two open-pit mines in Columbia with a history of spontaneous combustion events compiling a dataset with 21,000 entries. The logistic regression model revealed that the primary variables influencing the initiation of spontaneous combustion include seam temperature, atmospheric pressure, wind velocity, oxygen concentration, methane levels, altitude, ash content, volatile matter percentage, calorific value, vitrinite, liptinite, and the Hardgrove grindability index. Controlling certain variables can prevent the formation of conditions conducive to ignition. The key controllable factors are seam temperature, wind velocity, and oxygen concentration. Potential mitigation strategies involve sealing coal seams with materials that possess high thermal insulation and impermeability, as well as employing controlled blasting techniques such as precutting and buffer blasting to minimize heat transfer and restrict oxygen ingress, thereby inhibiting the oxidation reactions that promote combustion.

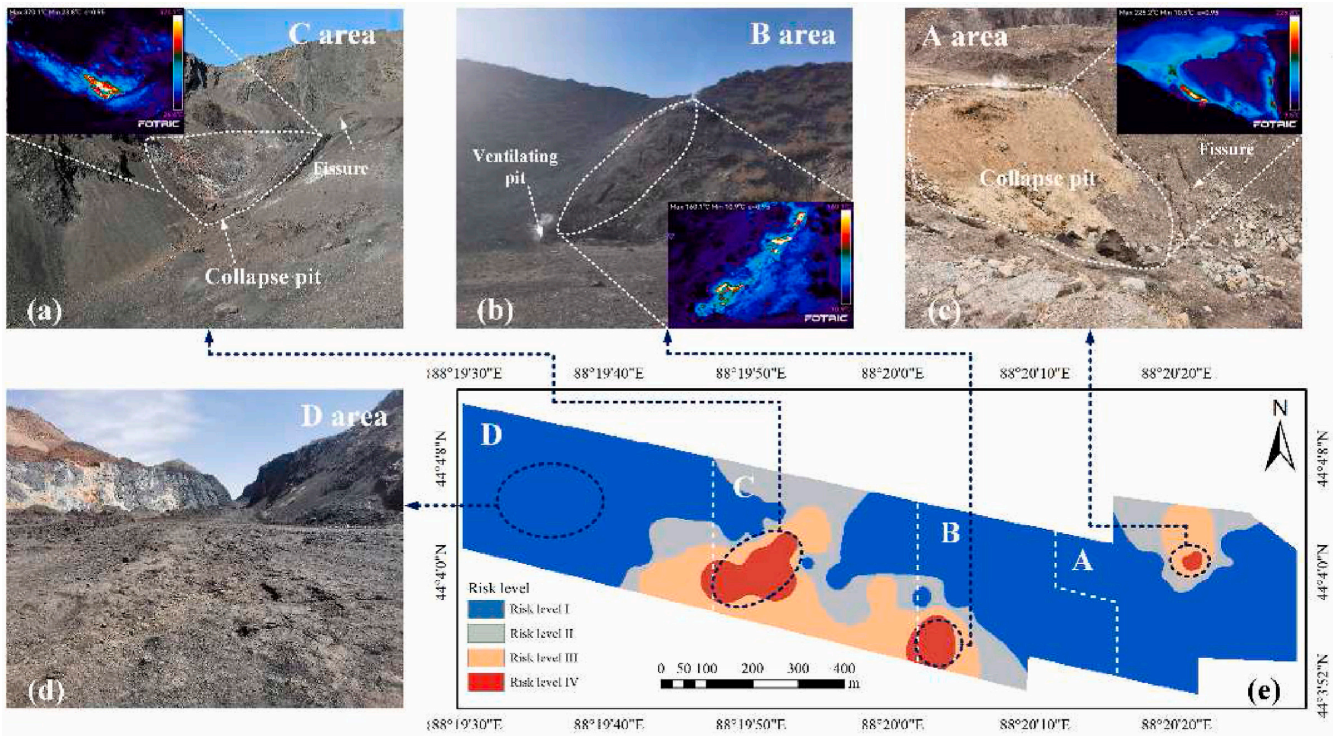

Figure 8. The results of the risk level assessment in four areas of the test region. (**a**) Field characteristics of area C; (**b**) field characteristics of area B; (**c**) field characteristics of area A; (**d**) field characteristics of area D; (**e**) risk level in the four areas considered. Reproduced from [135] with permission from Elsevier.

Abramovicz et al. [137] introduced and validated an innovative method for detecting subsurface smoldering fires by examining vegetation and soil condition changes in coal-waste dump areas affected by self-heating and spontaneous combustion. The study focused on the composition of plant species, life forms, and ecological groupings in relation to the heterogeneous particle size distribution of the deposited materials and fluctuating soil

temperatures. These factors significantly influenced the dynamics of vegetation, leading to the development of a distinct plant community. Notably, hemicryptophytes and apophytes were predominant in regions experiencing active thermal processes. The distribution of vegetation was monitored over three distinct periods along a transect that encompassed three surface categories with varying thermal characteristics and subsurface smoldering directions. Subsurface temperatures at a depth of 20 cm ranged from 9.9 °C to 139 °C, while surface temperatures varied from 3.1 °C to 69.0 °C. The total organic carbon (TOC) content across all samples was between 1.7% and 7.6%, with concentrations from 3.1% to 4.5% in areas of active fire. Total nitrogen levels were measured between 0.023% and 0.29%, and soil pH ranged from 5.8 to 8.0 when analyzed in water. Temporal and spatial variations in vegetation patterns were indicative of the progression of fire spots. The findings underscore the critical influence of subsurface temperatures on the spatial organization and species diversity of plant communities in coal-waste disposal sites affected by spontaneous combustion.

A similar approach was applied in an experimental study conducted by Ren et al. [138]. A spatial analysis method was proposed to achieve early warning spontaneous combustion of coal waste dump after reclamation by integrating unmanned aerial vehicle (UAV) and vegetation (Medicago sativa/alfalfa) growth status. The experiment was carried out in two slope areas of a coal waste dump after reclamation in Shanxi province, China, which were known for spontaneous combustion propensity. Three alfalfa growth parameters, aboveground biomass (AGB), plant water content (PWC), and plant height (PH) of the study area, were estimated from UAV imagery features and used to assess the spontaneous combustion risk. Then, soil deep temperature points (25 cm depth) distributed evenly in the study area were collected to determine the underground temperature situation. It was reported that the UAV-derived rededge Chlorophyll index (CIrededge), canopy temperature depression (CTD), and canopy height model (CHM) achieved a better estimation of alfalfa AGB (R^2 = 0.81, RMSE = 99.2 g/m^2, and MAE = 74.9 g/m^2), PWC (R^2 = 0.68, RMSE = 3.9%, and MAE = 3.2%), and PH (R^2 = 0.77, RMSE = 9.79 cm, and MAE = 7.68 cm) of the study area, respectively. Another key observation was that three alfalfa parameters were highly correlated with the soil deep temperature, but differed in degree (R^2 = 0.46–0.81). They were consistent with the soil deep temperature in spatial distribution and could reveal the change direction of underground temperature, which could be helpful to detect potential spontaneous combustion areas. These results indicated that vegetation is a prior indicator to the changes in underground temperature of coal waste dump.

Wang et al. [139] introduced a novel technique for evaluating the three-dimensional spatial distribution and oxidation status of coal gangue dump fire zones by correlating surface temperature data with gas and radon concentration measurements and analyzing their interdependencies. This technique enables the precise determination of the location, depth, spread, degree of oxidation, and potential evolution of combustion areas within coal gangue dumps. A specific methodology for assessing the depth and oxidation levels of the fires was formulated, involving the calculation of a depth index derived from the analysis of thermal fluctuations and radon dispersion patterns. The oxidation degree was quantified by identifying anomalies in radon emissions and surface temperature deviations and establishing diagnostic threshold values. The results obtained from the depth index and oxidation degree assessments were in agreement with the three-dimensional distribution analysis, providing a comprehensive approach for assessing the spontaneous combustion risk in coal gangue dump fire areas. This integrated framework enhances the understanding of the underlying processes that drive such fires, enabling more effective surveillance and mitigation strategies.

Surface and Integrated Techniques—Essential Conclusions and Research Needs

Surface and integrated techniques rely on the manifestations of subsurface combustion at the ground level. The primary advantage of these methods is that they do not require the deployment of equipment underground, allowing for the monitoring of extensive

areas with minimal instrumentation. Generally, these techniques are based on temperature measurements, typically obtained through infrared (IR) thermography and, less frequently, through direct contact sensors. For fires occurring below the surface, a notable change in surface temperature becomes detectable only after the fire has reached an advanced stage. However, surface measurement techniques offer other kind of qualitative information, which is not available in the case of other techniques. Propagation direction and speed can be easily assessed by means of surface temperature measurement techniques as well as a rough estimation of the fire size and trend, Song et al. [8]. During the early stages of coal seam combustion—specifically, low-temperature oxidation—the exothermic reactions do not produce sufficient thermal energy to cause a significant increase in surface temperature. Therefore, a combined approach, such as incorporating data from gas sensors, can provide early indications of the CSC state. Combined methodologies that integrate two or more independent detection techniques effectively mitigate the limitations of each individual method, resulting in a more robust and precise detection system. Data-driven methodologies, which utilize extensive datasets, offer a high level of generalizability. However, the effectiveness of the statistical algorithms used in these approaches is highly dependent on the quality of the data. While several studies have reported on data-driven methods, few have addressed issues related to data quality. Data quality encompasses aspects such as the data collection process, detection and removal of outliers, handling of missing values, bias control, stratification, and representativeness. Non-traditional techniques, such as soil and vegetation analysis, present some potential for the detection of CSC events. However, their effectiveness for timely and accurate identification remains limited, as they primarily assess the indirect effects of heat transfer from subsurface fires. Consequently, these techniques do not respond properly to the imperative of fast and accurate CSC detection in early stages.

5. Airborne and Spaceborne Techniques

5.1. Remote Sensing in Detection of CSC

Remote sensing is a pivotal technology in the field of Earth observation, employing advanced sensors mounted on satellite or aerial platforms to collect real-time data about the Earth's surface and atmosphere. Its applications span a wide range of disciplines, including environmental monitoring, land use mapping, and natural hazard assessment. In the context of detecting coal spontaneous combustion, remote sensing offers a unique advantage due to its ability to cover extensive areas, obtain data in real time, and penetrate through smoke or other obstructions using various spectral bands. Advanced techniques such as multispectral and hyperspectral imaging enable the identification of thermal anomalies and subtle changes in surface temperature, which are indicative of spontaneous combustion events in coal seams or stockpiles. Thermal infrared sensors, for example, can detect heat signatures that may not be apparent to the naked eye or standard optical instruments, allowing for early detection and mitigation of these hazardous events. Additionally, remote sensing can employ synthetic aperture radar to identify ground deformation associated with underground fires. By integrating remote sensing data with Geographic Information Systems and machine learning algorithms, it is possible to enhance the precision of combustion detection, forecast risk areas, and formulate effective intervention strategies. This multidisciplinary approach not only aids in preventing coal fire-related disasters but also contributes to minimizing associated environmental and economic impacts.

A comprehensive review by Syed et al. [140] focused on the remote sensing of coal fires in India, incorporating numerous studies related to fires in various regions across the country. The large volume of studies is attributed to the substantial losses caused by CSC events. Approximately 1.48 billion tons of coal remain unextracted due to around 70 surface and subsurface fires in the Jharia coalfield, a region that has been burning for over a century and spans an area of roughly 9 km^2. It is estimated that more than 37.6 million tons of coal have been consumed by fires in the Jharia coalfield alone. Based on the coal volume lost up to 2003 (37.6 million tons), the economic loss due to these fires, calculated using the 2018

import prices of coking and non-coking coal, is estimated to be around Rs. 280.74 billion. Several major research trends were identified as follows:

A. Thermal anomaly detection:
   A.1. Thermal IR sensors (TIR)
   A.2. Short-wave IR sensor (SWIR)
   A.3. Combined TIR and SWIR
B. Land subsidence monitoring
C. Geo-environmental indicators

This review critically analyzed the studies included and focused on limitations and shortcomings. Directions to improve the quality of observations and detection were identified and discussed, such as weighing factors—as spatial resolution, precision, detection potential, temporal constraints, and financial implications to determine the most suitable monitoring strategy. Integrating multiple techniques may provide a more effective solution by mitigating the drawbacks of each individual method. A discussion was included on how remote sensing could be employed to evaluate the CSC risk, develop fire mitigation strategies, and assessments of environmental impacts to comprehensively address the challenges posed by coal fire hazards.

Aerial monitoring of land for identification CSC is mainly based on IR thermal imaging. Thermal infrared (TIR) imaging is a remote sensing technique that identifies variations in the radiant energy emitted from the Earth's surface. Planck's law states that any object with a temperature above absolute zero (0 K) radiates energy in the thermal infrared range of the electromagnetic spectrum, making the primary challenge the accurate measurement of these variations. Fluctuations in radiant flux from the ground are primarily attributed to differences in the thermal properties of surface materials, such as rocks and soils, which affect their capacity to absorb solar radiation, retain it as heat (thermal capacity), and subsequently release it back into the atmosphere within the TIR spectrum. Several environmental and surface factors can influence radiant flux, thereby altering the tonal quality of TIR imagery. These include soil moisture content, the presence of bodies of water such as streams or wetlands, vertical stratification of vegetation (such as variations in tree canopy height), and active transpiration from dense vegetation areas, such as forests. Topographical features also play a significant role; for example, deep valleys may appear as warmer regions in TIR imagery due to reduced wind exposure or enhanced transpiration from vegetation. Additionally, large fauna, such as cattle or buffalo, may manifest as thermal anomalies or "hot spots" in TIR images, potentially leading to false positives in the interpretation of thermal data. Several recent studies on the CSC detection based on TIR imaging, discussing the hardware used and the processing algorithms, are presented in Table 6.

Color infrared (CIR) imaging employs modified color photographic film with altered spectral sensitivity, allowing it to capture reflected energy in the 0.7–0.9 μm range of the electromagnetic spectrum. A key advantage of CIR imaging is its capability to reveal the physiological condition of vegetation, often identifying signs of stress before they become apparent to an observer on the ground. Healthy vegetation, particularly in broadleaf forests, typically appears in various shades of red to magenta on CIR imagery, whereas stressed vegetation is represented by hues ranging from pink to blue, even when the stress is not yet visible to the naked eye. Vegetation in broadleaf forests can undergo stress due to a range of environmental factors, such as drought, disease, insect infestations, or other conditions that disrupt water uptake in the leaves. The capacity of CIR imaging to detect these early signs of stress has prompted its application in identifying the location and extent of coal fires. It has been hypothesized that the heat generated by a coal fire reduces the amount of water retained in the soil pores by surface tension. As a result, plants in the vicinity of a coal fire may progress more rapidly toward the wilting stage compared to those in unaffected areas. This differential stress response is detectable with CIR imaging, making it a valuable tool for early detection of coal fire impact zones.

Table 6. Hardware and processing approaches for CSC detection by means of TIR imaging.

Reference, Year	Platform	Sensor	Processing
Yuan et al. [141] 2021	UAV DJI M210 V2 drone with a Zenmuse XT 2 dual-light thermal infrared lens	TIR Resolution 640 × 512 TIR FOV: 32° × 26° RGB resolution: 4000 × 3000 RGB FOV: 57.12° × 42.44° TIR gain mode set to High, with the upper limit of the temperature range 150 °C	Two visual orthophotos (resolution of 2.54 cm) and two infrared images (resolution of 8.65 cm). The local variance and Shannon entropy are employed to explore the optimal observation scale and optimal coal fire area extraction scale for LST anomalies in coal fire areas.
Shao et al. [142] 2023	UAV DJI Matrice 210 RTK (Real-Time Kinematic) V2 quadrotor drone with a DJI Zenmuse XT2 dual-lens camera	12-megapixel RGB lens (FL: 8 mm, resolution: 4000 × 3000, pixel size 1.85 µm, FOV: 57.12° × 42.44°). FLIR Tau 2 IR lens (FL: 25 mm, TIR resolution 640 × 512, pixel size 17 µm, FOV: 25° × 20°). Temperature range: −25–135 °C (High gain); −40–550 °C (Low gain), thermal accuracy ±5 °C	The Rainbow High Contrast palette and temperature linear distribution mode were used to ensure that each image has a high contrast, color, and temperature consistency. Delineation and accurate identification of 3D temperature field were achieved by feature point matching and texture mapping.
Hu and Xia [71] 2017	TH9100MV/WV thermographic camera. RGB camera: Canon EOS 5D Mark digital camera for close range photogrammetry	TIR camera: 320 × 240 pixels and operates in the 8–14 µm range. The device has adjustable temperature measuring ranges from 0 °C to +500 °C with an accuracy of ±0.06 °C. RGB camera FL> 28 mm	Setting control points for the close-range photogrammetry. Setting the temperature-marked points (TMPs) for infrared thermograph. Bilinear interpolation algorithm provided the spatial coordinates and temperature values for each point in the grid.
He et al. [143] 2020	UAV DJI M210 Zenmuse XT2 cameras equipped with gimbal system	TIR camera: 640 × 512, 30 fps uncooled vanadium oxide (VOx) microbolometer for longwave radiation (7.5~13.5 µm); temperature range of −20 to 135 °C (high gain); FL 25 mm lens; File format raw 8-bit digital numbers; Acquisition rate: less than 9 Hz. RGB camera: 4K video, 12 megapixel photos	Maximum and minimum grey values of the TIR image were determined; based on the temperature range temperature anomaly regions were determined; coal fires and the locations of fire area were determined, with a ground resolution of 40 cm, corresponding to the pixel size.

Coal fires can induce alterations in the coloration of rock strata, degrade surrounding vegetation, release gases and smoke, and result in the accumulation of novel materials on the surface, Syed et al. [140]. Teodoro et al. [144] proposed a set of methodologies to monitor a decommissioned coal mine waste pile (São Pedro da Cova, Portugal) and its adjacent regions. Analysis of thermal and topographic data indicated a direct correlation between the temperature of the pile and ambient air temperature. However, in a localized area of approximately 200 m^2 near the base of the waste pile, spontaneous combustion was detected, with surface temperatures consistently exceeding 50 °C, irrespective of seasonal variations or fluctuations in air temperature. Land use and land cover (LULC) assessments, combined with the Normalized Difference Vegetation Index (NDVI) analysis, revealed that vegetation growth is confined to zones with comparatively lower surface temperatures. The presence of vegetation is critically important, as it plays a key role in mitigating soil erosion on the waste pile, thereby contributing to the stabilization of the structure. Additionally, a downward trend in altimetric measurements was observed, supporting the hypothesis that ongoing self-combustion processes are leading to a reduction in the volume of material within the waste pile. These findings underscore the complex interplay between thermal dynamics, vegetation cover, and topographical changes in areas affected

by coal waste combustion. The persistent thermal anomalies and the lack of vegetation in high-temperature zones highlight the challenges in achieving ecological restoration and physical stabilization of coal mine waste piles. The ongoing material depletion, as evidenced by the decreasing altimetric values, suggests that self-combustion continues to actively alter the waste pile's composition and structure, potentially posing risks to both the environment and surrounding communities.

Spaceborne remote sensing represents a powerful tool for the detection and monitoring of coal spontaneous combustion (CSC), offering several distinct advantages over traditional ground-based methods. Utilizing satellite-based platforms, this approach enables continuous, large-scale observation of the Earth's surface, providing consistent and comprehensive data coverage across vast and often inaccessible areas. The high temporal frequency and extensive spatial resolution afforded by spaceborne sensors facilitate the early identification of thermal anomalies associated with CSC, even in remote or hazardous environments. Specific advantages include the ability to capture multispectral and thermal infrared imagery, which is critical for detecting subtle changes in surface temperature and heat flux that indicate ongoing combustion processes. Furthermore, the integration of various spectral bands—from visible to thermal infrared—allows for the assessment of associated changes in surface characteristics, such as vegetation stress and ground deformation, which are indicative of subsurface fires. The ability to gather data across different wavelengths, combined with advanced data processing techniques, enhances the accuracy and reliability of CSC detection, making spaceborne remote sensing an indispensable component of modern environmental monitoring and risk management strategies.

Landsat 8 is a highly advanced Earth observation satellite launched in 2013 as part of the Landsat program, a long-standing initiative for remote sensing led by NASA and the United States Geological Survey (USGS). It carries two primary sensors: (i) the Operational Land Imager (push-broom sensor with a four-mirror telescope and 12-bit quantization, collecting data for visible, near infrared, and short wave infrared spectral bands as well as a panchromatic band). Such data are crucial for a range of applications including land use mapping, vegetation monitoring, and water resource management. (ii) Thermal Infrared Sensor (collecting data for two more narrow spectral bands in the thermal region formerly covered by one wide spectral band on Landsats 4–7). The TIRS provides data in two thermal infrared bands, enabling accurate surface temperature measurements essential for detecting heat anomalies like those caused by coal spontaneous combustion (CSC). Landsat 8's enhanced radiometric resolution (12-bit), moderate spatial resolution (30 m across most spectral bands), and regular revisit interval (every 16 days) establish it as a critical tool for remote sensing applications, providing consistent and high-quality data for monitoring environmental changes over extended periods. The open accessibility of Landsat 8 data further facilitates its extensive utilization in scientific research, environmental monitoring, and disaster response, including the identification of thermal anomalies linked to subsurface coal fires and other combustion events.

Song et al. [145] conducted a comprehensive in situ investigations of coal fires in order to assess the fire suppression efforts carried out in the Wuda syncline in May 2014, following an initial site visit to the Wuda coalfield in 2012. These field observations were combined with thermal anomaly data derived from Landsat-8 and Landsat-7 satellite imagery, using an automated moving-window thermal anomaly detection tool, known as the regional anomaly extractor. This integrated approach enabled a detailed analysis of coal fire behavior, considering the effects of fire-fighting interventions and the current state of combustion activity within the Wuda syncline.

When using data from IR satellite-based remote sensing systems, one of the problems faced is the correct classification of pixels in "fire" and "no-fire" classes. Roy et al. [133] conducted a study based on ASTER Level 1B thermal data (summer time) and Landsat-8 TIRS (winter time) with the aim of generating a coal fire map by selecting an optimal cut-off temperature using a statistically driven, data-centric approach. The cut-off temperature was identified through the examination of radiant temperature values from uniformly

distributed pixel clusters covering the entirety of the coal-bearing area. By employing this methodology, it was guaranteed that the selected cut-off temperature adequately addressed inherent variability and associated local complexities. Determining an appropriate cut-off temperature within thermal datasets to classify pixels into "fire" and "no fire" zones presents several challenges: the temperature of underlying terrain and background elements can exhibit significant seasonal fluctuations, and variations in the relative abundance of these elements across different sections of the coalfield may lead to inconsistencies in the cut-off temperature between sites. Additionally, the thermal contrast between active fire zones and surrounding areas, as captured in the remote sensing data, is highly dependent on factors such as the relative distribution of various rock types (e.g., sandstone, shale, and coal seams), land texture characteristics, the configuration of surface exposure (whether the fire is occurring at or beneath the surface), as well as the fire intensity and its spatial spread.

The algorithms used to process data from various satellite platforms are diverse but most of them employ the generalized single channel method, Jiménez-Muñoz and Sobrino [146] to determine the land surface temperature. The influence of atmosphere water content poses significant problems in processing the data. A selection of studies using data from Landsat, Sentinel, Envisat and ALOS PALSAR platforms and the data processing sequence is presented in Table 7. Techniques detecting landslides were also included in Table 7. These are even more complex than algorithms for land surface temperature determination.

Table 7. Typical algorithms for mapping the fire zones. LST and landslide detection studies.

Reference, Year	Remote Sensing Platform	Methodology	Objective Conclusions
Jiang et al. [147], 2017	Data before 2013: Landsat 5 Data after 2013: Landsat 7	Generalized single channel method (Jiménez-Muñoz and Sobrino [146] Planck's blackbody radiance law is divided by Taylor's Formula to obtain the approximate solution of land surface temperature). Natural breaks (Jenks [148]) clustering method was used to define four temperature classes. Eight scenes were selected including Landsat 5 and Landsat 7 images in the spring and fall from 2000 to 2015. (1) Radiance was calibrated using NASA calibration coefficients. (2) Geometric registration. (3) The FLAASH model was used to correct the atmosphere and obtained surface reflectance and moisture content. (4) Images were clipped for further processing.	Map the fire zone and assess the effectiveness of the CFSP (Coal Fire Suppression Project) over a period ranging from 2000 to 2015. CFSP successfully extinguished a significant percentage of surface area affected by coal fire while damaging the local landscape.
Wang et al. [149], 2022	Landsat 8	(1) Radiance correction and atmospheric correction were performed for multispectral data; the radiant brightness and brightness temperature of TIRS data are corrected to obtain the thermal radiation intensity value and the brightness temperature; (2) Terrain correction; (3) Calculation of surface emissivity; (4) Calculation of Atmospheric Water Vapor (AWV) based on NASA data on atmospheric transmissivity; (5) Generalized single channel method (Jiménez-Muñoz and Sobrino [146]) was used to determine the LST. Landsat-8 band 10 data were used for temperature inversion.	The average detection accuracy rate of the proposed method reaches 83.3%. The proposed coal fire detection approach can achieve good coal fire detection results regardless of using summer, winter, or annual data, with the annual data producing the best detection result.

Table 7. *Cont.*

Reference, Year	Remote Sensing Platform	Methodology	Objective Conclusions
Yu et al. [150], 2022	45 Landsat 8 images and 61 Sentinel-1 SAR images covering the same time span	(1) Utilizing the Radiative Transfer Equation (RTE) to retrieve land surface temperatures (LSTs) from multitemporal thermal infrared remote sensing data. (2) Normalizing the LSTs and applying an equidistant classification method to delineate thermal anomaly areas from remote sensing images obtained at various time intervals. (3) Quantifying the thermal anomaly frequencies (TAFs) across different regions. (4) Employing the Small Baseline Subset (SBAS) InSAR technique to derive temporal and spatial subsidence data. (5) Combining the mean subsidence values with the standard deviation to identify regions exhibiting significant subsidence within the study area. (6) Defining the threshold for thermal anomaly frequency (TAFT) by using land subsidence data as a constraint and designating an area as a coal fire zone if the observed frequency surpasses the TAFT. (7) Conducting a visual inspection of the results to eliminate any potential artificial heat sources. sources (such as industrial production areas) to further improve the identification accuracy.	To detect coal fire zones and evaluate their intensity and temporal evolution by integrating land surface temperature (LST) data, thermal anomaly metrics, and deformation information across a time series.
Jiang et al. [151], 2010	ENVISAT satellite (currently decommissioned), InSAR technique	A two-dimensional linear regression analysis of the differential interferometric phase was conducted on a set of 49 multi-master interferograms. The preliminary identification of Permanent Scatterers (PS) points was based on two selection criteria: (i) minimal temporal variability in the backscatter values, derived from co-registered Single Look Complex (SLC) intensity stacks, and (ii) the spectral characteristics of each individual SLC dataset.	The results obtained from InSAR analysis were cross-validated against GPS measurements acquired during two field campaigns in 2006 and 2008. A strong correlation was observed between the line-of-sight (LOS) displacement velocities derived from both methodologies, with an average absolute discrepancy of 5.4 mm/year and a standard deviation of 4.1 mm/year.
Mishra et al. [152], 2011	Landsat-7 ETM+ data of 29th March 2006 Ground data from TIR camera Jahria (India) of March, 2009	(1) Converting the image from digital number (DN) values to spectral radiance. (2) Transforming spectral radiance into radiant temperature. (3) Converting radiant temperature into surface temperature. The coal mine fire map derived from satellite imagery was categorized into three classifications: (i) Temperatures exceeding 52 °C were classified as high intensity, representing surface fires. (ii) Temperatures between 32 °C and 52 °C were identified as medium intensity, indicating subsurface fires. (iii) Temperatures at or below 32 °C were considered low intensity, corresponding to background or water bodies temperatures.	The discrepancy between surface temperature measurements and satellite-derived temperatures can be attributed to various factors, including wind direction and velocity, the angle and altitude of the thermal infrared (TIR) camera, atmospheric humidity, and the elevation of the terrain.

Table 7. *Cont.*

Reference, Year	Remote Sensing Platform	Methodology	Objective Conclusions
Biswal and Gorai [69], 2021	Landsat-5 (band 6) TM and Landsat-8 (band 10) Operational Land Imager/Thermal Infrared Sensor) satellite data of from 1989 to 2019.	(i) Landsat-8 sensor data were used for estimating the LST (Jiménez-Muñoz, J.C., Sobrino [146]) • Determination of atmospheric functions • Estimation of radiance • Estimation of LSE (ii) Determination of threshold LST for identifying the fire affected pixels (iii) Validation with ground temperature data	The fire-affected area measured 2.026, 3.009, 3.159, 3.991, 4.664, 8.656, and 9.957 km^2 for the years 1989, 1994, 1999, 2004, 2009, 2014, and 2019, respectively. The expansion of mining operations in the coalfield exposed additional coal seams to the atmosphere, leading to spontaneous heating and the formation of new coal fire pockets. Some fires were extinguished, either due to complete coal combustion or a cessation of the combustion process. The time-series analysis from 1989 to 2019 indicates both the formation of new fire pockets and the extinguishing of existing ones.
Zhou et al. [153], 2013	ALOS Phased Array type L-band Synthetic Aperture Radar	(i) Select pixels with coherence threshold (ii) Phase unwrapping for interferograms with short normal baselines (iii) Minimum Cost Flow method phase unwrapping (iv) Accumulated subsidence estimation (v) Average subsidence velocity calculation	Mean deformation rates of −8.52 cm/yr, −3.92 cm/yr, −4.6 cm/yr, −8.93 cm/yr and −6.07 cm/yr, were determined. Other areas outside the coal fire zones with similar subsidence signals were identified. Further investigation demonstrated that intense mining activities caused land subsidence in these areas.

5.2. Remote Sensing—Concluding Discussion

Remote sensing employs various sensors to acquire detailed information about objects and environments. It serves as an alternative to human-operated detection in inaccessible or hazardous areas, offering the advantage of rapidly collecting data with high spatial, spectral, and temporal resolution. Thermal infrared (TIR) data are particularly useful for detecting coal gangue pile fires, as it directly reflects surface temperature distribution. Remote sensing can be categorized into aerial and satellite-based methods, depending on the platform used.

Aerial remote sensing primarily involves color infrared or multispectral imaging, or the use of unmanned aerial vehicles (UAVs) equipped with TIR or hyperspectral sensors. Despite being influenced by factors such as surface albedo, terrain, and additional heat sources, these techniques provide high accuracy. Aerial methods detect surface features like thermal anomalies, heat-induced alterations in rock surfaces, and chemical byproducts of thermal processes. They are effective for large-area monitoring, such as coalfields, and hyperspectral imaging offers an additional advantage by correcting high-temperature saturation and sub-pixel issues. However, aerial surveillance is costly and impractical for continuous monitoring. In contrast, spaceborne remote sensing is more cost-effective and suitable for continuous, large-scale monitoring, particularly for tracking extensive coal fires and identifying fire propagation, Raju et al. [154], He et al. [155], Wang et al. [70], Singh et al. [156].

Spaceborne techniques employ three types of sensors: (i) multispectral sensors, such as those on the Landsat, MODIS, SPOT, and ASTER platforms, (ii) high spatial resolution sensors on platforms like Ikonos, Quickbird, and Worldview, and (iii) radar sensors. These sensors detect different features: multispectral sensors identify thermal anomalies, high spatial resolution sensors detect surface cracks and fissures, and radar sensors detect land subsidence and collapse. Radar methods, however, tend to have lower accuracy than multispectral and high-resolution techniques.

Very few studies exist though, attempting to integrate two or more remote sensing techniques, such as Elick [157] (thermal infrared imaging combined with CO/CO_2 measured along fire fronts to assess the progress and the fire depth). Karanam et al. [158] employed the methodology depicted in Figure 9 integrating thermal data from Landsat 8

and persistent Scatterer Interferometry analysis (60 Sentinel-1 C-band images) to monitor and map the coal fires in Jharia (India).

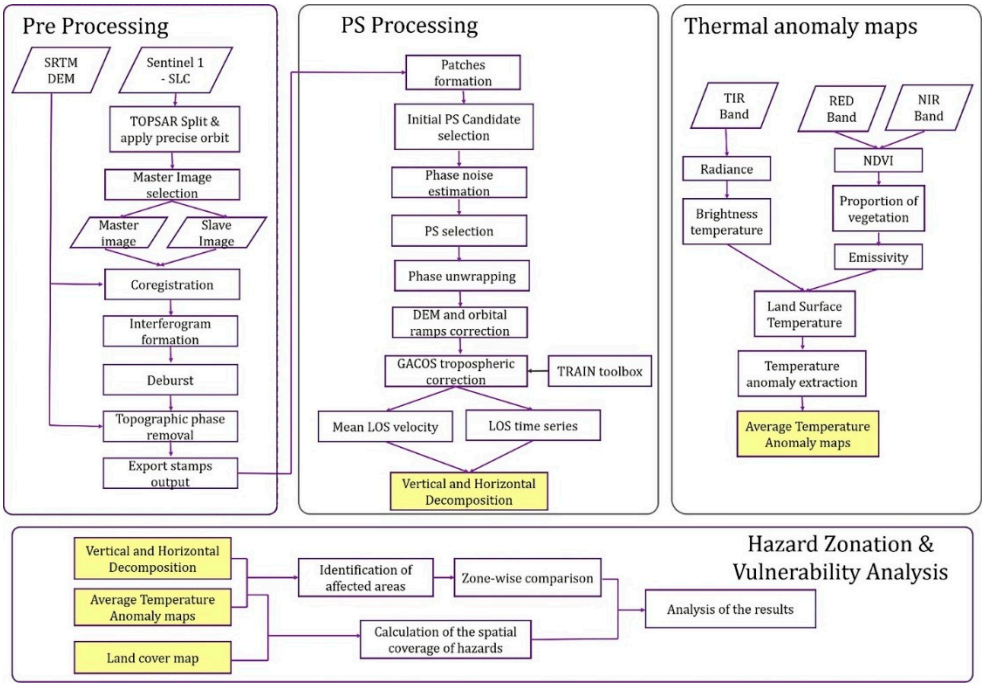

Figure 9. The methodology proposed by Karanam et al. [158] to combine TIR data with land subsidence information. Reproduced from [158] under CC BY 4.0.

6. Conclusions

The detection and monitoring of coal fires are critical for mapping their occurrence, modeling fire behavior, assessing environmental and public health impacts, and guiding fire-fighting engineering efforts. For instance, key model parameters such as fire depth, surface and subsurface temperatures, and fire propagation rates are fundamental inputs for computational simulations or serve as validation benchmarks for predictive models. These parameters also provide essential data for designing and implementing fire-fighting strategies. Additionally, monitoring emissions of greenhouse gases, toxic gases, and trace elements generated by coal fires is necessary for evaluating the environmental consequences and health risks posed by these fires.

The techniques discussed in this review can be broadly categorized into two main approaches: (i) the detection of coal spontaneous combustion (CSC) events during their initial stages, and (ii) the monitoring of fully developed fires—whether surface fires with visible flames or smoldering subsurface fires—to map their spatial extent, assess their progression, and evaluate the effectiveness of fire suppression interventions. From this review, several key observations and research directions can be identified to refine and narrow down CSC studies:

A. Site-Specificity of Detection Methods:

Many detection and monitoring methods are specifically designed or calibrated for particular coalfield sites, taking into account factors such as coal rank, composition, geological morphology, and climate. The literature lacks replication studies and discussions regarding the generalizability of these methods. This issue is particularly significant for early-stage CSC detection techniques, such as those targeting low-temperature oxidation. Experimental studies, whether conducted in the field or under controlled laboratory conditions, typically focus on specific types of coal and external conditions. Consequently, the accuracy and applicability of detection techniques designed for one site may not translate effectively to different locations with varying coal types and environmental factors.

B. Limitations of Laboratory-Controlled Experiments:

While laboratory-controlled experiments provide valuable insights, they cannot fully replicate the complex and dynamic conditions encountered at industrial coal sites. Real-world environments present numerous challenges, including variable gas emissions and absorption rates, fluctuating moisture levels, chemical spills, dust, noise, and other interfering factors. For instance, techniques such as thermal infrared imaging, though highly sensitive, may be overwhelmed by these environmental variables, limiting their practicality in industrial settings. There is a clear need for further research to bridge the gap between controlled laboratory findings and the realities of field conditions, ensuring that detection and monitoring techniques can be reliably applied in practical scenarios.

C. Development of Combined Techniques:

Although some progress has been made in developing ensemble or hybrid techniques that integrate multiple detection and monitoring approaches, these methods are still in their early stages. Combined techniques hold the potential to enhance robustness and accuracy by leveraging the strengths of individual methods while mitigating their weaknesses. For example, integrating thermal infrared imaging with gas detection sensors could improve the reliability of monitoring systems in variable environmental conditions. However, substantial research and development efforts are still required to advance these combined systems and validate their performance under real-world conditions.

In conclusion, while significant advancements have been made in the detection and monitoring of coal fires, several challenges remain. The site-specific nature of many techniques, the limitations of laboratory studies, and the early development of combined approaches all point to the need for further research to improve the accuracy, generalizability, and applicability of CSC detection and monitoring methods across diverse environments.

Author Contributions: Conceptualization, L..A and B.M.D.; methodology, L.A. and B.M.D.; formal analysis, B.M.D.; investigation, LA; resources, L.A.; data curation, L.A.; writing—original draft preparation, B.M.D.; writing—review and editing, B.M.D.; supervision, B.M.D.; All authors have read and agreed to the published version of the manuscript.

Funding: This research received no external funding.

Conflicts of Interest: The authors declare no conflict of interest.

References

1. Heffern, E.L.; Coates, D.A. Geologic history of natural coal-bed fires, Powder River basin, USA. *Int. J. Coal Geol.* **2004**, *59*, 25–47. [CrossRef]
2. Song, Z.; Zhu, H.; Jia, G.; He, C. Comprehensive evaluation on self-ignition risks of coal stockpiles using fuzzy AHP approaches. *J. Loss Prev. Process. Ind.* **2014**, *32*, 78–94. [CrossRef]
3. Liu, H.; Hong, R.; Xiang, C.; Lv, C.; Li, H. Visualization and analysis of mapping knowledge domains for spontaneous combustion studies. *Fuel* **2019**, *262*, 116598. [CrossRef]
4. Yang, F.; Qiu, D. Exploring coal spontaneous combustion by bibliometric analysis. *Process. Saf. Environ. Prot.* **2019**, *132*, 1–10. [CrossRef]
5. Huang, Z.; Ma, Z.; Song, S.; Yang, R.; Gao, Y.; Zhang, Y. Study on the influence of periodic weighting on the spontaneous combustion "three-zone" in a gob. *J. Loss Prev. Process. Ind.* **2018**, *55*, 480–491. [CrossRef]
6. Onifade, M.; Genc, B. A review of research on spontaneous combustion of coal. *Int. J. Min. Sci. Technol.* **2020**, *30*, 303–311. [CrossRef]
7. Zhang, J.; Ren, T.; Liang, Y.; Wang, Z. A review on numerical solutions to self-heating of coal stockpile: Mechanism, theoretical basis, and variable study. *Fuel* **2016**, *182*, 80–109. [CrossRef]
8. Song, Z.; Kuenzer, C. Coal fires in China over the last decade: A comprehensive review. *Int. J. Coal Geol.* **2014**, *133*, 72–99. [CrossRef]
9. Lu, X.; Deng, J.; Xiao, Y.; Zhai, X.; Wang, C.; Yi, X. Recent progress and perspective on thermal-kinetic, heat and mass transportation of coal spontaneous combustion hazard. *Fuel* **2022**, *308*, 121234. [CrossRef]
10. Li, Q.-W.; Xiao, Y.; Zhong, K.-Q.; Shu, C.-M.; Lü, H.-F.; Deng, J.; Wu, S. Overview of commonly used materials for coal spontaneous combustion prevention. *Fuel* **2020**, *275*, 117981. [CrossRef]
11. Onifade, M. Countermeasures against coal spontaneous combustion: A review. *Int. J. Coal Prep. Util.* **2021**, *42*, 2953–2975. [CrossRef]
12. Kong, B.; Li, Z.; Yang, Y.; Liu, Z.; Yan, D. A review on the mechanism, risk evaluation, and prevention of coal spontaneous combustion in China. *Environ. Sci. Pollut. Res.* **2017**, *24*, 23453–23470. [CrossRef] [PubMed]

13. Han, D.; Niu, G.; Zhu, H.; Chang, T.; Liu, B.; Ren, Y.; Wang, Y.; Song, B. Exploration and Frontier of Coal Spontaneous Combustion Fire Prevention Materials. *Processes* **2024**, *12*, 1155. [CrossRef]
14. Lu, W.; Cao, H.; Sun, X.; Hu, X.; Li, J.; Li, J.; Kong, B. A Review on the Types, Performance and Environmental Protection of Filling & Plugging Materials for Prevention and Control of Coal Spontaneous Combustion in China. *Combust. Sci. Technol.* **2022**, *196*, 2299–2335. [CrossRef]
15. Dai, J.; Tian, Z.-J.; Shi, X.-Y.; Lu, Y.; Chi, W.-L.; Zhang, Y. Research progress on gravity heat pipe technology to prevent spontaneous combustion in coal storage piles. *MRS Commun.* **2024**, *14*, 480–488. [CrossRef]
16. Kuenzer, C.; Zhang, J.; Sun, Y.; Jia, Y.; Dech, S. Coal fires revisited: The Wuda coal field in the aftermath of extensive coal fire research and accelerating extinguishing activities. *Int. J. Coal Geol.* **2012**, *102*, 75–86. [CrossRef]
17. Saini, V.; Gupta, R.P.; Arora, M.K. Environmental impact studies in coalfields in India: A case study from Jharia coal-field. *Renew. Sustain. Energy Rev.* **2015**, *53*, 1222–1239. [CrossRef]
18. Kuenzer, C.; Stracher, G.B. Geomorphology of coal seam fires. *Geomorphology* **2012**, *138*, 209–222. [CrossRef]
19. Kus, J. Impact of underground coal fire on coal petrographic properties of high volatile bituminous coals: A case study from coal fire zone No. 3.2 in the Wuda Coalfield, Inner Mongolia Autonomous Region, North China. *Int. J. Coal Geol.* **2017**, *171*, 185–211. [CrossRef]
20. Xu, Y.; Uhl, D.; Zhang, N.; Zhao, C.; Qin, S.; Liang, H.; Sun, Y. Evidence of widespread wildfires in coal seams from the Middle Jurassic of Northwest China and its impact on paleoclimate. *Palaeogeogr. Palaeoclim. Palaeoecol.* **2020**, *559*, 109819. [CrossRef]
21. Li, C.; Sun, J.; Shi, J.; Liang, H.; Cao, Q.; Li, Z.; Gao, Y. Mercury sources in a subterranean spontaneous combustion area. *Ecotoxicol. Environ. Saf.* **2020**, *201*, 110863. [CrossRef] [PubMed]
22. Carroll, M.; Gao, C.X.; Campbell, T.C.; Smith, C.L.; Dimitriadis, C.; Berger, E.; Maybery, D.; Ikin, J.; Abramson, M.J.; Sim, M.R.; et al. Impacts of coal mine fire-related PM2.5 on the utilisation of ambulance and hospital services for mental health conditions. *Atmos. Pollut. Res.* **2022**, *13*, 101415. [CrossRef]
23. Oliveira, M.L.; Pinto, D.; Tutikian, B.F.; da Boit, K.; Saikia, B.K.; Silva, L.F. Pollution from uncontrolled coal fires: Continuous gaseous emissions and nanoparticles from coal mines. *J. Clean. Prod.* **2019**, *215*, 1140–1148. [CrossRef]
24. Deng, J.; Ge, S.; Qi, H.; Zhou, F.; Shi, B. Underground coal fire emission of spontaneous combustion, Sandaoba coalfield in Xinjiang, China: Investigation and analysis. *Sci. Total. Environ.* **2021**, *777*, 146080. [CrossRef] [PubMed]
25. Xia, T.; Zhou, F.; Liu, J.; Kang, J.; Gao, F. A fully coupled hydro-thermo-mechanical model for the spontaneous combustion of underground coal seams. *Fuel* **2014**, *125*, 106–115. [CrossRef]
26. Rúa, M.O.B.; Aragón, A.J.D.; Baena, P.B. A study of fire propagation in coal seam with numerical simulation of heat transfer and chemical reaction rate in mining field. *Int. J. Min. Sci. Technol.* **2019**, *29*, 873–879. [CrossRef]
27. Xi, Z.; Suo, L.; Xia, T. Characterization of elementary reactions inducing coal spontaneous combustion. *Fuel* **2024**, *358*, 130138. [CrossRef]
28. Xiao, Y.; Ren, S.-J.; Deng, J.; Shu, C.-M. Comparative analysis of thermokinetic behavior and gaseous products between first and second coal spontaneous combustion. *Fuel* **2018**, *227*, 325–333. [CrossRef]
29. Yuan, H.; Restuccia, F.; Richter, F.; Rein, G. A computational model to simulate self-heating ignition across scales, configurations, and coal origins. *Fuel* **2019**, *236*, 1100–1109. [CrossRef]
30. Taraba, B.; Michalec, Z.; Michalcová, V.; Blejchař, T.; Bojko, M.; Kozubková, M. CFD simulations of the effect of wind on the spontaneous heating of coal stockpiles. *Fuel* **2014**, *118*, 107–112. [CrossRef]
31. Rong-Kun, P.; Chang, L.; Ke, Y.; Ming-Gao, Y. Distribution Regularity and Numerical Simulation Study on the Coal Spontaneous Combustion "three zones" Under the Ventilation Type of Ventilation Type of Ч + J. *Procedia Eng.* **2011**, *26*, 704–711. [CrossRef]
32. Zhuo, H.; Qin, B.; Qin, Q.; Su, Z. Modeling and simulation of coal spontaneous combustion in a gob of shallow buried coal seams. *Process. Saf. Environ. Prot.* **2019**, *131*, 246–254. [CrossRef]
33. Xiaomeng, L.; Minbo, Z.; Xiaoyan, Z.; Bo, T.; Saiyi, G. Numerical-simulation study on the influence of wind speed and segregation effect on spontaneous combustion of coal bunker. *Case Stud. Therm. Eng.* **2023**, *52*, 103678. [CrossRef]
34. Zhang, J.; Choi, W.; Ito, T.; Takahashi, K.; Fujita, M. Modelling and parametric investigations on spontaneous heating in coal pile. *Fuel* **2016**, *176*, 181–189. [CrossRef]
35. Yu, M.; Yang, N.; Li, H.; Wang, L.; Wu, M.; Wang, F.; Chu, T.; Wang, K. Numerical investigation on the effects of axial-stress loads on the temperature-programmed oxidation characteristics of loose broken coal. *Energy* **2024**, *289*, 129974. [CrossRef]
36. Plakunov, M.; Yavuzturk, C.; Chiasson, A. On the effects of temperature-dependent diffusion of carbon dioxide from underground coal fires. *Geothermics* **2020**, *85*, 101768. [CrossRef]
37. Qiao, L.; Deng, C.; Lu, B.; Wang, Y.; Wang, X.; Deng, H.; Zhang, X. Study on calcium catalyzes coal spontaneous combustion. *Fuel* **2022**, *307*, 121884. [CrossRef]
38. Deng, B.; Qiao, L.; Wang, Y.; Mu, X.; Deng, C.; Jin, Z. Study on the effect of inorganic and organic sodium on coal spontaneous combustion. *Fuel* **2023**, *353*, 129256. [CrossRef]
39. Zhang, Y.; Luo, Y.; Amini, S.H. Systematic investigation on the effect of particle size on low-rank coal spontaneous combustion under various extrinsic conditions. *Fuel* **2023**, *334*, 126844. [CrossRef]
40. Zhang, J.; Liang, Y.; Ren, T.; Wang, Z.; Wang, G. Transient CFD modelling of low-temperature spontaneous heating behaviour in multiple coal stockpiles with wind forced convection. *Fuel Process. Technol.* **2016**, *149*, 55–74. [CrossRef]

41. Li, D.-J.; Xiao, Y.; Lü, H.-F.; Xu, F.; Liu, K.-H.; Shu, C.-M. Effects of 1-butyl-3-methylimidazolium tetrafluoroborate on the exothermic and heat transfer characteristics of coal during low-temperature oxidation. *Fuel* **2020**, *273*, 117589. [CrossRef]
42. Said, K.O.; Onifade, M.; Lawal, A.I.; Githiria, J.M. An Artificial Intelligence-based Model for the Prediction of Spontaneous Combustion Liability of Coal Based on Its Proximate Analysis. *Combust. Sci. Technol.* **2020**, *193*, 2350–2367. [CrossRef]
43. Lei, C.; Deng, J.; Cao, K.; Xiao, Y.; Ma, L.; Wang, W.; Ma, T.; Shu, C. A comparison of random forest and support vector machine approaches to predict coal spontaneous combustion in gob. *Fuel* **2019**, *239*, 297–311. [CrossRef]
44. Sahu, H.; Mahapatra, S.; Sirikasemsuk, K.; Panigrahi, D. A discrete particle swarm optimization approach for classification of Indian coal seams with respect to their spontaneous combustion susceptibility. *Fuel Process. Technol.* **2011**, *92*, 479–485. [CrossRef]
45. Xie, Z.; Zhang, Y.; Jin, C. Prediction of Coal Spontaneous Combustion in Goaf Based on the BP Neural Network. *Procedia Eng.* **2012**, *43*, 88–92. [CrossRef]
46. Li, S.; Ma, X.; Yang, C. Prediction of spontaneous combustion in the coal stockpile based on an improved metabolic grey model. *Process Saf. Environ. Prot.* **2018**, *116*, 564–577. [CrossRef]
47. Sahu, H.; Padhee, S.; Mahapatra, S. Prediction of spontaneous heating susceptibility of Indian coals using fuzzy logic and artificial neural network models. *Expert Syst. Appl.* **2010**, *38*, 2271–2282. [CrossRef]
48. Wang, K.; Li, K.; Du, F.; Zhang, X.; Wang, Y.; Sun, J. Research on prediction model of coal spontaneous combustion temperature based on SSA-CNN. *Energy* **2024**, *290*, 130158. [CrossRef]
49. Li, J.; Fu, P.; Zhu, Q.; Mao, Y.; Yang, C. A lab-scale experiment on low-temperature coal oxidation in context of underground coal fires. *Appl. Therm. Eng.* **2018**, *141*, 333–338. [CrossRef]
50. Onifade, M.; Genc, B.; Carpede, A. A new apparatus to establish the spontaneous combustion propensity of coals and coal-shales. *Int. J. Min. Sci. Technol.* **2018**, *28*, 649–655. [CrossRef]
51. Wen, H.; Wang, H.; Liu, W.; Cheng, X. Comparative study of experimental testing methods for characterization parameters of coal spontaneous combustion. *Fuel* **2020**, *275*, 117880. [CrossRef]
52. Zhang, H.; Wang, Y.; Zhang, X.; Sasaki, K.; Sugai, Y.; Han, F.; Dong, W.; Thanh, H.V. Experimental study of moisture effects on spontaneous combustion of Baiyinhua lignite from individual particles to stockpile. *Fuel* **2023**, *334*, 126774. [CrossRef]
53. Yan, H.; Nie, B.; Liu, P.; Chen, Z.; Yin, F.; Gong, J.; Lin, S.; Wang, X.; Kong, F.; Hou, Y. Experimental investigation and evaluation of influence of oxygen concentration on characteristic parameters of coal spontaneous combustion. *Thermochim. Acta* **2022**, *717*, 179345. [CrossRef]
54. Zhao, J.; Yang, X.; Song, J.; Zhang, Y.; Shu, C.-M. Experimental study of coal spontaneous combustion high-temperature region spreading characteristics. *Process. Saf. Environ. Prot.* **2023**, *180*, 136–147. [CrossRef]
55. Fan, X.-L.; Ma, L.; Sheng, Y.-J.; Liu, X.-X.; Wei, G.-M.; Liu, S.-M. Experimental investigation on the characteristics of XG/GG/HPAM gel foam and prevention of coal spontaneous combustion. *Energy* **2023**, *284*, 128710. [CrossRef]
56. Zhang, Y.; Xu, J.; Wang, D. Experimental Study on the Inhibition Effects of Nitrogen and Carbon Dioxide on Coal Spontaneous Combustion. *Energies* **2020**, *13*, 5256. [CrossRef]
57. Zhang, X.; Gui, Y.; Lu, B.; Bai, G.; Qiao, L.; Li, C.; Zhang, X.; Gui, Y.; Lu, B.; Bai, G.; et al. Experimental study on the effect of inhibitor on coal spontaneous combustion under low temperature freezing. *Fuel* **2024**, *365*, 131225. [CrossRef]
58. Cheng, J.; Ma, Y.; Wang, C.; Wang, W.; Zhang, L.; Hu, X.; Zhang, M.; Ma, Z. A novel cement-based flexible spray coating for flame retardant. *Process. Saf. Environ. Prot.* **2023**, *177*, 366–379. [CrossRef]
59. Liu, Y.; Wen, H.; Guo, J.; Jin, Y.; Wei, G.; Yang, Z. Coal spontaneous combustion and N2 suppression in triple goafs: A numerical simulation and experimental study. *Fuel* **2020**, *271*, 117625. [CrossRef]
60. Tang, Y.; Hou, F.; Zhong, X.; Huang, A.; Jia, X.; Peng, B. Combination of heat energy extraction and fire control in underground high-temperature zones of coal fire areas. *Energy* **2023**, *278*, 127801. [CrossRef]
61. Hu, X.; Yang, S.; Zhou, X.; Yu, Z.; Hu, C. Coal spontaneous combustion prediction in gob using chaos analysis on gas indicators from upper tunnel. *J. Nat. Gas Sci. Eng.* **2015**, *26*, 461–469. [CrossRef]
62. Du, B.; Liang, Y.; Tian, F. Detecting concealed fire sources in coalfield fires: An application study. *Fire Saf. J.* **2021**, *121*, 103298. [CrossRef]
63. Wei, D.; Du, C.; Lei, B.; Lin, Y. Prediction and prevention of spontaneous combustion of coal from goafs in workface: A case study. *Case Stud. Therm. Eng.* **2020**, *21*, 100668. [CrossRef]
64. Ma, L.; Zou, L.; Ren, L.-F.; Chung, Y.-H.; Zhang, P.-Y.; Shu, C.-M. Prediction indices and limiting parameters of coal spontaneous combustion in the Huainan mining area in China. *Fuel* **2020**, *264*, 116883. [CrossRef]
65. Guo, J.; Wen, H.; Zheng, X.; Liu, Y.; Cheng, X. A method for evaluating the spontaneous combustion of coal by monitoring various gases. *Process. Saf. Environ. Prot.* **2019**, *126*, 223–231. [CrossRef]
66. Guo, J.; Shang, H.; Cai, G.; Jin, Y.; Wang, K.; Li, S. Early Detection of Coal Spontaneous Combustion by Complex Acoustic Waves in a Concealed Fire Source. *ACS Omega* **2023**, *8*, 16519–16531. [CrossRef]
67. Gao, R.; Zhu, H.; Liao, Q.; Qu, B.; Hu, L.; Wang, H. Detection of coal fire by deep learning using ground penetrating radar. *Measurement* **2022**, *201*, 111585. [CrossRef]
68. Zhou, B.; Wu, J.; Wang, J.; Wu, Y. Surface-based radon detection to identify spontaneous combustion areas in small abandoned coal mine gobs: Case study of a small coal mine in China. *Process. Saf. Environ. Prot.* **2018**, *119*, 223–232. [CrossRef]
69. Biswal, S.S.; Gorai, A.K. Studying the coal fire dynamics in Jharia coalfield, India using time-series analysis of satellite data. *Remote. Sens. Appl. Soc. Environ.* **2021**, *23*, 100591. [CrossRef]

70. Wang, Y.-J.; Tian, F.; Huang, Y.; Wang, J.; Wei, C.-J. Monitoring coal fires in Datong coalfield using multi-source remote sensing data. *Trans. Nonferrous Met. Soc. China* **2015**, *25*, 3421–3428. [CrossRef]
71. Hu, Z.; Xia, Q. An integrated methodology for monitoring spontaneous combustion of coal waste dumps based on surface temperature detection. *Appl. Therm. Eng.* **2017**, *122*, 27–38. [CrossRef]
72. Kong, B.; Wang, E.; Lu, W.; Li, Z. Application of electromagnetic radiation detection in high-temperature anomalous areas experiencing coalfield fires. *Energy* **2019**, *189*, 116144. [CrossRef]
73. Liu, W.; Qin, Y.; Yang, X.; Wang, W.; Chen, Y. Early extinguishment of spontaneous combustion of coal underground by using dry-ice's rapid sublimation: A case study of application. *Fuel* **2018**, *217*, 544–552. [CrossRef]
74. Shi, X.; Zhang, C.; Jin, P.; Zhang, Y.; Jiao, F.; Xu, S.; Cao, W. Eliminating scale effect: Development and attenuation of coal spontaneous combustion. *Fuel* **2024**, *357*, 130073. [CrossRef]
75. Zhai, X.; Wu, S.; Wang, K.; Drebenstedt, C.; Zhao, J. Environment influences and extinguish technology of spontaneous combustion of coal gangue heap of Baijigou coal mine in China. *Energy Procedia* **2017**, *136*, 66–72. [CrossRef]
76. Cheng, W.; Hu, X.; Xie, J.; Zhao, Y. An intelligent gel designed to control the spontaneous combustion of coal: Fire prevention and extinguishing properties. *Fuel* **2017**, *210*, 826–835. [CrossRef]
77. Cheng, J.; Wu, Y.; Dong, Z.; Zhang, R.; Wang, W.; Wei, G.; Chu, T.; Yu, Z.; Qin, Y.; Liu, G.; et al. A novel composite inorganic retarding gel for preventing coal spontaneous combustion. *Case Stud. Therm. Eng.* **2021**, *28*, 101648. [CrossRef]
78. Fan, Y.-J.; Zhao, Y.-Y.; Hu, X.-M.; Wu, M.-Y.; Xue, D. A novel fire prevention and control plastogel to inhibit spontaneous combustion of coal: Its characteristics and engineering applications. *Fuel* **2020**, *263*, 116693. [CrossRef]
79. Li, Y.; Xiao, G.; Li, F.; Guo, Y.; Chen, C.; Chen, C.; Li, R.; Yang, Z. A novel H-TiO_2/gel co-stabilized three-dimensional network synergistic fire-retardant foam gel for coal-pile. *Colloids Surf. A Physicochem. Eng. Asp.* **2022**, *650*, 129642. [CrossRef]
80. Shi, B.; Su, H.; Li, J.; Qi, H.; Zhou, F.; Torero, J.L.; Chen, Z. Clean Power Generation from the Intractable Natural Coalfield Fires: Turn Harm into Benefit. *Sci. Rep.* **2017**, *7*, 5302. [CrossRef]
81. Su, H.; Zhou, F.; Qi, H.; Li, J. Design for thermoelectric power generation using subsurface coal fires. *Energy* **2017**, *140*, 929–940. [CrossRef]
82. Xiao, Y.; Yin, L.; Tian, Y.; Li, S.-G.; Zhai, X.-W.; Shu, C.-M.; Ren, S.-J. Sustainable utilisation and transformation of the thermal energy from coalfield fires: A comprehensive review. *Appl. Therm. Eng.* **2023**, *233*, 121164. [CrossRef]
83. Xiao, Y.; Gao, L.-H.; Meng, X.; Liu, J.-W.; Lu, X.; Tian, Y.; Shu, C.-M. Thermal removal from coal fires by a two-phase closed thermosyphon with a CuO nanofluid. *Case Stud. Therm. Eng.* **2023**, *42*, 102745. [CrossRef]
84. Liang, Y.; Zhang, J.; Wang, L.; Luo, H.; Ren, T. Forecasting spontaneous combustion of coal in underground coal mines by index gases: A review. *J. Loss Prev. Process. Ind.* **2018**, *57*, 208–222. [CrossRef]
85. Dong, X.; Wen, Z.; Wang, F.; Meng, Y. Law of gas production during coal heating oxidation. *Int. J. Min. Sci. Technol.* **2019**, *29*, 617–620. [CrossRef]
86. Xueqiu, H.; Xianfeng, L.; Baisheng, N.; Dazhao, S. FTIR and Raman spectroscopy characterization of functional groups in various rank coals. *Fuel* **2017**, *206*, 555–563. [CrossRef]
87. Zhao, J.; Deng, J.; Wang, T.; Song, J.; Zhang, Y.; Shu, C.-M.; Zeng, Q. Assessing the effectiveness of a high-temperature-programmed experimental system for simulating the spontaneous combustion properties of bituminous coal through thermokinetic analysis of four oxidation stages. *Energy* **2018**, *169*, 587–596. [CrossRef]
88. Cliff, D.; Davis, R.; Bennet, T.; Galvin, G.; Clarksosn, F. Large Scale Laboratory Testing of the Spontaneous Combustibility of Australian Coals. Queensland Mining Industry Health and Safety Conference Proceedings. 1998. Available online: https://www.osti.gov/etdeweb/biblio/296307 (accessed on 23 August 2024).
89. Xie, J.; Xue, S.; Cheng, W.; Wang, G. Early detection of spontaneous combustion of coal in underground coal mines with development of an ethylene enriching system. *Int. J. Coal Geol.* **2010**, *85*, 123–127. [CrossRef]
90. Qing, G.; Wanxing, R.; Wei, L. Risk evaluation of coal spontaneous combustion from the statistical characteristics of index gases. *Thermochim. Acta* **2022**, *715*, 179287. [CrossRef]
91. Ma, T.; Zhai, X.-W.; Xiao, Y.; Bai, Y.-E.; Shen, K.; Song, B.-B.; Hao, L.; Ren, L.-F.; Chen, X.-K. Study on the influence of key active groups on gas products in spontaneous combustion of coal. *Fuel* **2023**, *344*, 128020. [CrossRef]
92. Yang, S.; Hu, X.; Liu, W.V.; Cai, J.; Zhou, X. Spontaneous combustion influenced by surface methane drainage and its prediction by rescaled range analysis. *Int. J. Min. Sci. Technol.* **2018**, *28*, 215–221. [CrossRef]
93. MDG 1006 Spontaneous Combustion Management—Technical Reference. Available online: https://www.resourcesregulator.nsw.gov.au/ (accessed on 21 August 2024).
94. Liu, H.; Li, Z.; Li, J.; Yang, Y.; Zhang, Y. CO-based early warning threshold for coal spontaneous combustion. *Mater. Chem. Phys.* **2024**, *313*, 128730. [CrossRef]
95. Xu, Y.-L.; Liu, Z.-J.; Wang, L.-Y.; Lv, Z.-G.; Wu, J.-D.; Li, M.-J. Hysteresis characteristics of oxidation-thermodynamic for residual coal in goaf under uniaxial stress. *Fuel* **2021**, *306*, 121750. [CrossRef]
96. Danish, E.; Onder, M. Application of Fuzzy Logic for Predicting of Mine Fire in Underground Coal Mine. *Saf. Health Work.* **2020**, *11*, 322–334. [CrossRef] [PubMed]
97. Singh, A.K.; Singh, R.; Singh, M.P.; Chandra, H.; Shukla, N. Mine fire gas indices and their application to Indian underground coal mine fires. *Int. J. Coal Geol.* **2006**, *69*, 192–204. [CrossRef]

98. Yan, H.; Nie, B.; Liu, P.; Chen, Z.; Yin, F.; Gong, J.; Lin, S.; Wang, X.; Kong, F.; Hou, Y. Experimental assessment of multi-parameter index gas correlation and prediction system for coal spontaneous combustion. *Combust. Flame* **2023**, *247*, 112485. [CrossRef]
99. Lu, H.; Li, J.; Lu, W.; Xu, Z.; Li, J.; He, Q. Variation laws of CO2/CO and influence of key active groups on it during low-temperature oxidation of coal. *Fuel* **2023**, *339*, 127415. [CrossRef]
100. Wang, C.-P.; Deng, Y.; Zhang, Y.-T.; Xiao, Y.; Deng, J.; Shu, C.-M. Coal oxidation characteristics and index gases of spontaneous combustion during the heating and cooling processes. *Fuel* **2022**, *307*, 121806. [CrossRef]
101. Li, L.; Ren, T.; Zhong, X.; Wang, J. Study of ambient temperature oxidation in low metamorphic coal and the oxidation mechanism. *Energy* **2022**, *252*, 124039. [CrossRef]
102. Liu, H.; Wang, F.; Ren, T.; Qiao, M.; Yan, J. Influence of methane on the prediction index gases of coal spontaneous combustion: A case study in Xishan coalfield, China. *Fuel* **2020**, *289*, 119852. [CrossRef]
103. Zhang, D.; Cen, X.; Wang, W.; Deng, J.; Wen, H.; Xiao, Y.; Shu, C.-M. The graded warning method of coal spontaneous combustion in Tangjiahui Mine. *Fuel* **2020**, *288*, 119635. [CrossRef]
104. Cheng, J.; Ma, Y.; Lu, W.; Liu, G.; Cai, F. Using inverting CO critical value to predict coal spontaneous combustion severity in mine gobs with considering air leakages—A case study. *Process. Saf. Environ. Prot.* **2022**, *167*, 45–55. [CrossRef]
105. Chang, G.; Chang, H. Underground abnormal sensor condition detection based on gas monitoring data and deep learning image feature engineering. *Heliyon* **2023**, *9*, e22026. [CrossRef] [PubMed]
106. Marwan, N.; Carmenromano, M.; Thiel, M.; Kurths, J. Recurrence plots for the analysis of complex systems. *Phys. Rep.* **2007**, *438*, 237–329. [CrossRef]
107. Lu, Z.; Zhou, B.; Wang, J.; Chan, Z.; Yang, Q.; Dong, Z.; Dong, K. Study on the formation mechanism of a radon source during coal spontaneous combustion in a goaf. *Fuel* **2023**, *336*, 127135. [CrossRef]
108. Zhou, B.; Deng, C.; Hao, J.; An, B.; Wu, R. Experimental study on the mechanism of radon exhalation during coal spontaneous combustion in goaf. *Tunn. Undergr. Space Technol.* **2021**, *113*, 103776. [CrossRef]
109. Wen, H.; Xiaojiao, C.; Yanhui, X.; Li, M.; Jun, G.; Kiyin, J.; Baoqi, W.; Junchang, J. Law of radon precipitation and migration in loose coal during spontaneous combustion process. *J. China Coal Soc.* **2019**, *44*, 9. [CrossRef]
110. Chan, Z.; Zhou, B.; Wang, J.; Lu, Z.; Yang, Q.; Dong, Z.; Dong, K. Long-distance migration law of radon in overburden of abandoned goaf during coal spontaneous combustion. *J. Environ. Radioact.* **2023**, *270*, 107284. [CrossRef]
111. Wen, H.; Cheng, X.; Fan, S.; Xu, Y.; Ren, S.; Guo, J. A method for detecting hidden fire source in deep mine goafs based on radon measurement and its experimental verification. *Appl. Geochem.* **2020**, *117*, 104603. [CrossRef]
112. Ding, W.-C.; He, L.; Huang, H.-Q.; Xu, W.-F.; Li, S.-B.; He, T. Study on alpha cup technique for monitoring of soil radon levels. *J. Radioanal. Nucl. Chem.* **2017**, *314*, 1635–1641. [CrossRef]
113. Hu, X.; Sun, Q.; Shi, Q.; Wang, N.; Geng, J.; Xue, S. Radon exhalation characteristics after pyrolysis of long flame coal. *Sci. Total. Environ.* **2023**, *904*, 167228. [CrossRef]
114. Gbadamosi, A.; Onifade, M.; Genc, B.; Rupprecht, S. Analysis of spontaneous combustion liability indices and coal recording standards/basis. *Int. J. Min. Sci. Technol.* **2020**, *30*, 723–736. [CrossRef]
115. de Boer, C.B.; Dekkers, M.J.; van Hoof, T.A. Rock-magnetic properties of TRM carrying baked and molten rocks straddling burnt coal seams. *Phys. Earth Planet. Inter.* **2001**, *126*, 93–108. [CrossRef]
116. Kong, B.; Li, Z.; Wang, E.; Lu, W.; Chen, L.; Qi, G. An experimental study for characterization the process of coal oxidation and spontaneous combustion by electromagnetic radiation technique. *Process. Saf. Environ. Prot.* **2018**, *119*, 285–294. [CrossRef]
117. Wang, E.; He, X.; Liu, X.; Li, Z.; Wang, C.; Xiao, D. A non-contact mine pressure evaluation method by electromagnetic radiation. *J. Appl. Geophys.* **2011**, *75*, 338–344. [CrossRef]
118. Kong, G.; Zhou, L.; Peng, H.; Gu, H. Reduction rate of dragload and downdrag of piles by taper angles. *Trans. Tianjin Univ.* **2016**, *22*, 434–440. [CrossRef]
119. Kong, B.; Wang, E.; Li, Z.; Niu, Y. Time-varying characteristics of electromagnetic radiation during the coal-heating process. *Int. J. Heat Mass Transf.* **2017**, *108*, 434–442. [CrossRef]
120. Kong, B.; Wang, E.; Li, Z. Regularity and coupling correlation between acoustic emission and electromagnetic radiation during rock heating process. *Geomech. Eng.* **2018**, *15*, 1125–1133. [CrossRef]
121. Zhu, H.; Qu, B.; Liao, Q.; Xie, L.; Wang, J.; Hu, L.; Wang, H.; Gao, R. Evolution and mechanism for the terahertz dielectric spectrum of coal during oxidation. *Infrared Phys. Technol.* **2022**, *127*, 104412. [CrossRef]
122. Zhu, H.; Wang, W.; Wang, H.; Zhao, H.; Xin, M. Study on electrical properties of coal at spontaneous combustion characteristic temperature. *J. Appl. Geophys.* **2018**, *159*, 707–714. [CrossRef]
123. Karaoulis, M.; Revil, A.; Mao, D. Localization of a coal seam fire using combined self-potential and resistivity data. *Int. J. Coal Geol.* **2014**, *128-129*, 109–118. [CrossRef]
124. Shi, X.; Wu, K. Research and Application of Comprehensive Electromagnetic Detection Technique in Spontaneous Combustion Area of Coalfields. *Procedia Earth Planet. Sci.* **2011**, *3*, 195–202. [CrossRef]
125. Ren, S.-J.; Zhang, Y.-N.; Song, Z.-Y.; Xiao, Y.; Deng, J.; Shu, C.-M. Initial exploration on potential fire hazards detection from coal spontaneous combustion applied by acoustic wave. *Sci. Total. Environ.* **2023**, *897*, 165475. [CrossRef] [PubMed]
126. Deng, J.; Qu, G.; Ren, S.; Wang, C.; Xiao, Y.; Wang, J.; Sa, B.; Duan, X.; Yang, N.; Zhao, X. Investigation on high temperature point detection of spontaneous combustion of loose coal based on optimal acoustic signal. *Process. Saf. Environ. Prot.* **2024**, *185*, 423–434. [CrossRef]

127. Kong, B.; Zhong, J.; Wei, J.; Lu, W.; Sun, X.; Yang, G.; Zhao, X.; Ma, L. Study on sound wave kinematic characteristics and temperature sensing mechanism during the warming process of loose coals. *Energy* **2024**, *307*, 132753. [CrossRef]
128. Liu, J.; Ma, Y.; Kong, B.; Bing, Y.; Yang, T.; Zhao, X.; Ma, L. Study on the precursor characteristics of coal energy spontaneous combustion process using infrasound wave monitoring and warning. *Energy* **2024**, *292*, 130406. [CrossRef]
129. Ide, T.S.; Crook, N.; Orr, F. Magnetometer measurements to characterize a subsurface coal fire. *Int. J. Coal Geol.* **2011**, *87*, 190–196. [CrossRef]
130. Shao, Z.; Wang, D.; Wang, Y.; Zhong, X. Theory and application of magnetic and self-potential methods in the detection of the Heshituoluogai coal fire, China. *J. Appl. Geophys.* **2014**, *104*, 64–74. [CrossRef]
131. Pandey, J.; Kumar, D.; Mishra, R.K.; Mohalik, N.K.; Khalkho, A.; Singh, V.K. Application of Thermography Technique for Assessment and Monitoring of Coal Mine Fire: A Special Reference to Jharia Coal Field, Jharkhand, India. *Int. J. Adv. Remote Sens.* **2013**, *2*, 138–147.
132. Misz-Kennan, M.; Tabor, A. The Thermal History of Select Coal-Waste Dumps in the Upper Silesian Coal Basin, Poland. In *Coal and Peat Fires: A Global Perspective*; Stracher, G.B., Prakash, A., Sokol, E.V., Eds.; Elsevier Inc.: Amsterdam, The Netherlands, 2015; Volume 3, pp. 432–462. [CrossRef]
133. Roy, P.; Guha, A.; Kumar, K.V. An approach of surface coal fire detection from ASTER and Landsat-8 thermal data: Jharia coal field, India. *Int. J. Appl. Earth Obs. Geoinf.* **2015**, *39*, 120–127. [CrossRef]
134. Wang, H.; Fang, X.; Li, Y.; Zheng, Z.; Shen, J. Research and application of the underground fire detection technology based on multi-dimensional data fusion. *Tunn. Undergr. Space Technol.* **2020**, *109*, 103753. [CrossRef]
135. Wang, H.; Fan, C.; Chen, L.; Chen, X.; Zhang, J.; Zhong, H. Research on early identification of burning status in a fire area in Xinjiang based on data-driven. *Case Stud. Therm. Eng.* **2024**, *60*, 104685. [CrossRef]
136. Rúa, M.B.; Aragón, A.D.; Baena, P.B.; Botero, J.O. Statistical analysis to establish an ignition scenario based on extrinsic and intrinsic variables of coal seams that affect spontaneous combustion. *Int. J. Min. Sci. Technol.* **2019**, *29*, 731–737. [CrossRef]
137. Abramowicz, A.; Rahmonov, O.; Chybiorz, R.; Ciesielczuk, J. Vegetation as an indicator of underground smoldering fire on coal-waste dumps. *Fire Saf. J.* **2021**, *121*, 103287. [CrossRef]
138. Ren, H.; Zhao, Y.; Xiao, W.; Zhang, J.; Chen, C.; Ding, B.; Yang, X. Vegetation growth status as an early warning indicator for the spontaneous combustion disaster of coal waste dump after reclamation: An unmanned aerial vehicle remote sensing approach. *J. Environ. Manag.* **2022**, *317*, 115502. [CrossRef]
139. Wang, H.; Fang, X.; Du, F.; Tan, B.; Zhang, L.; Li, Y.; Xu, C. Three-dimensional distribution and oxidation degree analysis of coal gangue dump fire area: A case study. *Sci. Total. Environ.* **2021**, *772*, 145606. [CrossRef]
140. Syed, T.H.; Riyas, M.J.; Kuenzer, C. Remote sensing of coal fires in India: A review. *Earth-Sci. Rev.* **2018**, *187*, 338–355. [CrossRef]
141. Yuan, G.; Wang, Y.; Zhao, F.; Wang, T.; Zhang, L.; Hao, M.; Yan, S.; Dang, L.; Peng, B. Accuracy assessment and scale effect investigation of UAV thermography for underground coal fire surface temperature monitoring. *Int. J. Appl. Earth Obs. Geoinf.* **2021**, *102*, 102426. [CrossRef]
142. Shao, Z.; Deng, R.; Zhang, G.; Li, Y.; Tang, X.; Zhang, W. 3D thermal mapping of smoldering coal gangue pile fires using airborne thermal infrared data. *Case Stud. Therm. Eng.* **2023**, *48*, 103146. [CrossRef]
143. He, X.; Yang, X.; Luo, Z.; Guan, T. Application of unmanned aerial vehicle (UAV) thermal infrared remote sensing to identify coal fires in the Huojitu coal mine in Shenmu city, China. *Sci. Rep.* **2020**, *10*, 13895. [CrossRef]
144. Teodoro, A.; Santos, P.; Marques, J.E.; Ribeiro, J.; Mansilha, C.; Melo, A.; Duarte, L.; de Almeida, C.R.; Flores, D. An Integrated Multi-Approach to Environmental Monitoring of a Self-Burning Coal Waste Pile: The São Pedro da Cova Mine (Porto, Portugal) Study Case. *Environments* **2021**, *8*, 48. [CrossRef]
145. Song, Z.; Kuenzer, C.; Zhu, H.; Zhang, Z.; Jia, Y.; Sun, Y.; Zhang, J. Analysis of coal fire dynamics in the Wuda syncline impacted by fire-fighting activities based on in-situ observations and Landsat-8 remote sensing data. *Int. J. Coal Geol.* **2015**, *141–142*, 91–102. [CrossRef]
146. Jiménez-Muñoz, J.C.; Sobrino, J.A. A generalized single-channel method for retrieving land surface temperature from remote sensing data. *J. Geophys. Res. Atmos.* **2003**, *108*, D22. [CrossRef]
147. Jiang, W.; Jia, K.; Chen, Z.; Deng, Y.; Rao, P. Using spatiotemporal remote sensing data to assess the status and effectiveness of the underground coal fire suppression efforts during 2000–2015 in Wuda, China. *J. Clean. Prod.* **2017**, *142*, 565–577. [CrossRef]
148. Jenks, G.F. The data model concept in statistical mapping. *Int. Yearb. Cartogr.* **1967**, *7*, 186–190.
149. Wang, T.; Wang, Y.; Zhao, F.; Feng, H.; Liu, J.; Zhang, L.; Zhang, N.; Yuan, G.; Wang, D. A spatio-temporal temperature-based thresholding algorithm for underground coal fire detection with satellite thermal infrared and radar remote sensing. *Int. J. Appl. Earth Obs. Geoinf.* **2022**, *110*, 102805. [CrossRef]
150. Yu, B.; She, J.; Liu, G.; Ma, D.; Zhang, R.; Zhou, Z.; Zhang, B. Coal fire identification and state assessment by integrating multitemporal thermal infrared and InSAR remote sensing data: A case study of Midong District, Urumqi, China. *ISPRS J. Photogramm. Remote. Sens.* **2022**, *190*, 144–164. [CrossRef]
151. Jiang, L.; Lin, H.; Ma, J.; Kong, B.; Wang, Y. Potential of small-baseline SAR interferometry for monitoring land subsidence related to underground coal fires: Wuda (Northern China) case study. *Remote. Sens. Environ.* **2010**, *115*, 257–268. [CrossRef]
152. Mishra, R.; Bahuguna, P.; Singh, V. Detection of coal mine fire in Jharia Coal Field using Landsat-7 ETM+ data. *Int. J. Coal Geol.* **2011**, *86*, 73–78. [CrossRef]

153. Zhou, L.; Zhang, D.; Wang, J.; Huang, Z.; Pan, D. Mapping Land Subsidence Related to Underground Coal Fires in the Wuda Coalfield (Northern China) Using a Small Stack of ALOS PALSAR Differential Interferograms. *Remote. Sens.* **2013**, *5*, 1152–1176. [CrossRef]
154. Raju, A.; Singh, A.; Chandniha, S.K. A synergetic approach for quantification and analysis of coal fires in Jharia Coalfield, India. *Phys. Chem. Earth Parts A/B/C* **2023**, *131*, 103441. [CrossRef]
155. He, D.; Le, B.T.; Xiao, D.; Mao, Y.; Shan, F.; Ha, T.T.L. Coal mine area monitoring method by machine learning and multispectral remote sensing images. *Infrared Phys. Technol.* **2019**, *103*, 103070. [CrossRef]
156. Singh, N.; Chatterjee, R.; Kumar, D.; Panigrahi, D. Spatio-temporal variation and propagation direction of coal fire in Jharia Coalfield, India by satellite-based multi-temporal night-time land surface temperature imaging. *Int. J. Min. Sci. Technol.* **2021**, *31*, 765–778. [CrossRef]
157. Elick, J.M. Mapping the coal fire at Centralia, Pa using thermal infrared imagery. *Int. J. Coal Geol.* **2011**, *87*, 197–203. [CrossRef]
158. Karanam, V.; Motagh, M.; Garg, S.; Jain, K. Multi-sensor remote sensing analysis of coal fire induced land subsidence in Jharia Coalfields, Jharkhand, India. *Int. J. Appl. Earth Obs. Geoinf.* **2021**, *102*, 102439. [CrossRef]